Available online at www.sciencedirect.com

ScienceDirect

Geochimica et Cosmochimica Acta 308 (2021) 273–290

Geochimica et Cosmochimica Acta

www.elsevier.com/locate/gca

Origins and implications of magnesium isotopic heterogeneity in Fe–Ti oxides in layered mafic intrusions

Lie-Meng Chen [a,*], Fang-Zhen Teng [b,*], Xie-Yan Song [a], Yan Luan [c], Song-Yue Yu [a], Jian Kang [a,d]

[a] State Key Laboratory of Ore Deposit Geochemistry, Institute of Geochemistry, Chinese Academy of Sciences, Guiyang 550081, China
[b] Isotope Laboratory, Department of Earth and Space Sciences, University of Washington, Seattle, Washington 98195, USA
[c] School of Earth Science and Resources, Chang'an University, Xi'an 710054, China
[d] University of Chinese Academy of Sciences, Beijing 100049, China

Received 1 October 2020; accepted in revised form 9 June 2021; available online 15 June 2021

Abstract

To constrain the mechanisms governing the extremely large variations of Mg and Fe isotopes in magmatic Fe–Ti oxides in layered mafic intrusions, we investigate Mg isotopic compositions of magnetite, coupled with its chemical data and whole-rock major element and Sr-Nd isotope compositions from the Baima layered mafic intrusion in the Emeishan large igneous province, SW China. The Baima intrusion is mainly composed of magnetite-wehrlite and magnetite-troctolite (i.e., oxide-rich rocks) in the Lower Zone, and troctolite and gabbro (i.e., oxide-barren rocks) in the Middle and Upper Zones. Magnetite separates display large Mg isotopic variation, with δ^{26}Mg ranging from -0.17 ± 0.06 to $+0.58 \pm 0.04$‰ in the oxide-rich rocks and from -0.18 ± 0.06 to $+0.98 \pm 0.04$‰ in the oxide-barren ones. The lack of correlation of δ^{26}Mg with trace elements in magnetite and whole-rock Sr-Nd isotopic compositions indicates that the large Mg isotopic variation in magnetite was not produced by fractional crystallization, magma mixing, crustal contamination, and/or trapped liquid shift. Instead, equilibrium isotope fractionation induced by Mg–Fe re-equilibration between magnetite and ilmenite at different subsolidus temperatures controlled the Mg isotopic variation in the oxide-rich rocks; and kinetic isotope fractionation driven by Mg–Fe inter-diffusion between magnetite and olivine and/or clinopyroxene dominated the oxide-barren rocks. Both processes were primarily controlled by the assemblage and modal abundance of coexisting minerals to which magnetite adjoins. Overall, fractional crystallization and subsequent subsolidus diffusion played crucial roles in the genesis of the Fe–Ti oxides in the Baima intrusion. Our results also reveal widespread isotope disequilibrium between coexisting minerals in mafic magma chambers and suggest that Mg isotope geochemistry has a great potential to characterize the formation of Fe–Ti oxides in layered mafic intrusions.

Keywords: Magnesium isotopes; Magnetite; Isotope fractionation; Diffusion; Subsolidus processes; Layered mafic intrusions

1. INTRODUCTION

Magnetite and ilmenite (i.e., Fe–Ti oxides) are two widespread Mg-Fe-bearing phases in igneous rocks on the Earth and the Moon (Frost and Lindsley, 1991). Investigation of non-traditional stable isotope compositions, such as Mg and Fe isotopes, of Fe–Ti oxides in igneous rocks may provide important insights into the processes of magmatic evolution and the petrogenesis of layered mafic intrusions (Sossi et al., 2012; Chen et al., 2014, 2018; Dziony et al., 2014; Liu et al., 2014a; Bilenker et al., 2017; Cao et al., 2019; Teng et al., 2019; Tian et al., 2020). For example,

* Corresponding authors.
E-mail addresses: chenliemeng@vip.gyig.ac.cn (L.-M. Chen), fteng@u.washington.edu (F.-Z. Teng).

https://doi.org/10.1016/j.gca.2021.06.016
0016-7037/

Mg and Fe isotopic compositions of Fe–Ti oxides shed light on the processes of lunar magma ocean (LMO) differentiation, as the lunar high-Ti and low-Ti basalts have distinct isotopic compositions (Fig. 1; Sedaghatpour et al., 2013; Sossi and O'Neill, 2017; Sedaghatpour and Jacobsen, 2018). Recently, large Mg isotopic variations have been documented in Fe–Ti oxides in layered mafic intrusions, with δ^{26}Mg ranging from −0.80 to +23.10‰ in ilmenite (Chen et al., 2018; Tian et al., 2020), which is much larger than the mantle (−0.25 ± 0.04‰), global mid-ocean ridge basalts (MORBs, from −0.31 to −0.19‰), and silicate minerals (Fig. 1a; Teng, 2017, and references therein). Similarly, δ^{57}Fe of magnetite and ilmenite vary from −0.49 to +1.27‰ and from −0.99 to +0.07‰ in igneous rocks, respectively (Sossi et al., 2012; Chen et al., 2014; Dziony et al., 2014; Liu et al., 2014a; Bilenker et al., 2017; Cao et al., 2019; Knipping et al., 2019; Tian et al., 2020; Wei et al., 2020), much greater than global MORBs (from +0.06 to +0.35‰) (Fig. 1b; Teng et al., 2013; Zhao et al., 2015; Chen et al., 2019; Gleeson et al., 2020).

To date, the mechanisms governing the large Mg and Fe isotopic variations in Fe–Ti oxides in layered mafic intrusions are still highly debated. Based on mineral proportions and compositions, Chen et al. (2014, 2018) proposed that the large variations of Mg isotopes in ilmenite and Fe isotopes in Fe–Ti oxides at the Baima intrusion (China) resulted from Mg–Fe (and Ti) exchange between ilmenite and magnetite/ferromagnesian silicates (i.e., olivine and clinopyroxene) during cooling of the magma chamber. Similar interpretations were also used to explain Fe isotope fractionation between magnetite and ilmenite in the Skaergaard intrusion (Greenland) and Bushveld Complex (South Africa) (Dziony et al., 2014; Bilenker et al., 2017). Alternatively, Liu et al. (2014a, 2014b) and Cao et al. (2019) suggested that *in-situ* crystallization of immiscible Fe- and Si-rich melts controlled the disequilibrium Fe isotope fractionation between Fe–Ti oxides and ferromagnesian silicates at the Baima and Panzhihua intrusions (China). More recently, Tian et al. (2020) reported extremely large Mg and Fe isotopic variations in ilmenite at Panzhihua, which were interpreted as a result of Mg–Fe inter-diffusion between ilmenite and interstitial immiscible melts. These different mechanisms responsible for Mg and Fe isotopic variations in Fe–Ti oxides are associated with different geological processes and have different implications in the genesis of Fe–Ti oxides in layered mafic intrusions.

One of the key reasons leading to the above debate is the lack of Mg isotopic data for magnetite that coexists with ilmenite. Magnetite and ilmenite generally coexist in terrestrial igneous rocks and are expected to experience extensive inter-mineral exchanges of Mg–Fe–Ti during cooling (Pang et al., 2008b, and references therein). Coupled Mg isotope studies of both magnetite and ilmenite thus may help to constrain the mechanisms and processes governing Mg and Fe isotopic variations and the origins of Fe–Ti oxides in layered mafic intrusions. To date, Mg isotopic compositions of magnetite are still absent.

Here, we present for the first time Mg isotopic compositions of magnetite, coupled with its chemical data and whole-rock major element and Sr-Nd isotope compositions from the Baima layered mafic intrusion (Fig. S1). We found large Mg isotopic variations in magnetite, with δ^{26}Mg ranging from −0.18 ± 0.06 to +0.98 ± 0.04‰, reflecting both equilibrium and kinetic isotope fractionations among magnetite, ilmenite, and ferromagnesian silicates during subsolidus processes. Our results suggest that fractional crystallization and subsolidus inter-mineral interactions play essential roles in the formation of Fe–Ti oxides in layered mafic intrusions.

2. GEOLOGICAL BACKGROUND

Several mafic–ultramafic layered intrusions hosting giant Fe–Ti oxide ore deposits, including Baima, Panzhihua, Taihe, Hongge, and Xinjie occur in the central zone of the Emeishan large igneous province, SW China (Panxi

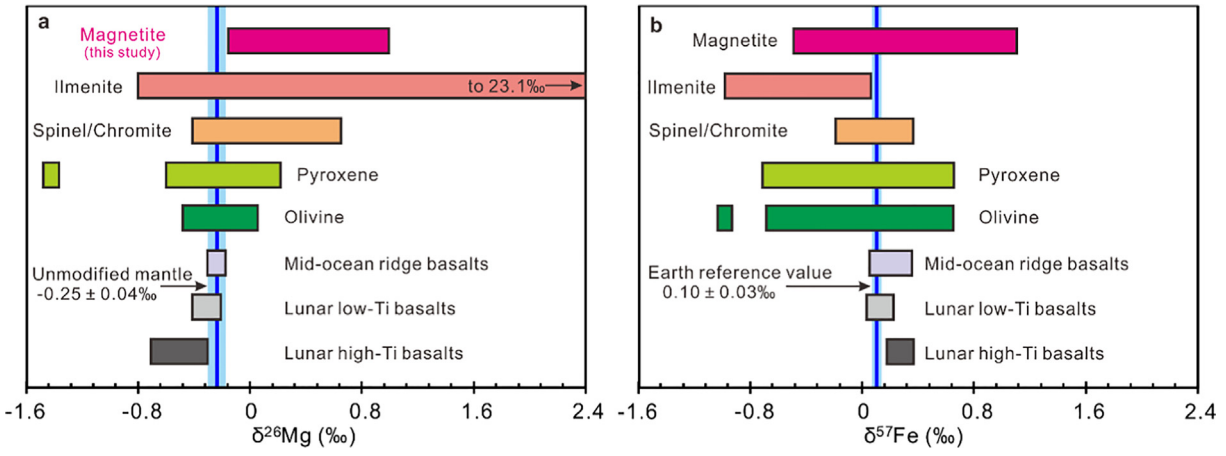

Fig. 1. (a) Mg and (b) Fe isotopic distributions of the Earth, Moon, silicate minerals, and Fe–Ti oxides. Data sources of δ^{26}Mg are from this study, Teng (2017), Chen et al. (2018), Sedaghatpour and Jacobsen (2018), and Tian et al. (2020). Data sources of δ^{57}Fe (including published δ^{57}Fe values and re-calculated data from δ^{56}Fe) are from Teng et al. (2011), Chen et al. (2014), Liu et al. (2014a, 2014b), Dziony et al. (2014), Zhao et al. (2015), Bilenker et al., (2017), Cao et al. (2019), Chen et al. (2019), Knipping et al. (2019), Poitrasson, et al. (2019), Gleeson et al. (2020), Tian et al. (2020), and Wei et al. (2020). The vertical blue line and bars represent (a) the average Mg isotopic value of the mantle (−0.25 ± 0.04‰, Teng et al., 2010) and (b) the Earth reference value (0.10 ± 0.03‰, Poitrasson et al., 2019).

Geological Unit, 1984). These intrusions were emplaced at ~260 Ma and were genetically associated with the high-Ti basaltic magmatism of the Emeishan mantle plume (Fig. S1) (Xu et al., 2004; Zhou et al., 2008). The geology and petrography of the Baima intrusion have been reported extensively in previous studies (Panxi Geological Unit, 1984; Shellnutt et al., 2009; Shellnutt and Pang, 2012; Zhang et al., 2012; Zhang et al., 2013; Chen et al., 2014, 2018; Liu et al., 2014a, 2014b), and only a summary is provided below.

The N–S striking Baima intrusion, ~24 km long and ~1.5–6.0 km thick, is one of the representative layered mafic intrusions (Panxi Geological Unit, 1984). It comprises predominately magnetite-wehrlite and magnetite-troctolite (defined as oxide-rich rocks hereafter, >30 wt% $Fe_2O_{3(T)}$ in whole rocks) in the Lower Zone and troctolite and gabbro (defined as oxide-barren rocks hereafter, <30 wt% $Fe_2O_{3(T)}$ in whole rocks) in the Middle and Upper Zones (Fig. S1; Chen et al., 2014).

The oxide-rich rocks are characterized by abundant cumulates of Fe–Ti oxides (up to 70 modal%), olivine, plagioclase, and clinopyroxene, coupled with minor inter-cumulus minerals of hornblende and base metal sulfides (Panxi Geological Unit, 1984; Chen et al., 2014). Medium-to-coarse grained magnetite crystals are mainly in contact with each other and/or ilmenite (Fig. S2), displaying straight to slightly curved edges and/or ~120° triple junctions. Besides, magnetite crystals host abundant exsolution lamellae of ilmenite and spinel (Zhang et al., 2012).

The oxide-barren rocks are rich in cumulus minerals of clinopyroxene, plagioclase, and olivine, coupled with small amounts of inter-cumulus Fe–Ti oxides (<20 modal%), hornblende, and/or apatite (Panxi Geological Unit, 1984; Chen et al., 2014). Fine-to-medium grained magnetite commonly adjoins ferromagnesian silicates and/or ilmenite (Fig. S2). Magnetite crystals in the oxide-barren rocks contain much fewer exsolution lamellae of ilmenite than those in the oxide-rich ones. Additionally, micro-texture observations suggest that all Fe–Ti oxides and silicate minerals are fresh with limited hydrothermal alteration (Zhang et al., 2012; Chen et al., 2014, 2018).

3. SAMPLES AND ANALYTICAL METHODS

Cumulate rocks were sampled from the Lower, Middle, and Upper Zones of the Baima intrusion (Fig. S1). All samples were crushed to cm-sized fragments and subdivided into three groups: (1) the first group was powdered for whole-rock major element and Sr–Nd isotope analyses, (2) the second was polished to make thin sections for *in-situ* chemical analyses, and (3) the last was crushed to 120–180 μm for mineral separation.

Magnetite grains were first handpicked under a binocular microscope, then demagnetized via heating to ~550 °C, and checked several times under a binocular microscope at 50x magnification to ensure a visible purity of ~100%. The purified magnetite separates were finally cleaned in Milli-Q water before chemical digestion for Mg isotope analyses.

3.1. Whole-rock major element and Sr–Nd isotope analyses

Whole-rock major element compositions were analyzed by X ray fluorescence spectrometer (XRF) at ALS Chemex Co., Ltd (Guangzhou, China). Ferrous oxide analyses were determined by titrimetry. The estimated precision varied from <2% relative standard deviation for major elements (e.g., Si, Mg, Fe, Al, and Ca) to <7% for minor elements (e.g., Mn, Ti, Na, and K).

Whole-rock Sr–Nd isotopic analyses were performed using a Thermofisher Triton multi-collector thermal ionization mass spectrometer (TIMS) at State Key Laboratory of Ore Deposit Geochemistry, Institute of Geochemistry, Chinese Academy of Sciences. Whole-rock powders (~120 mg) were dissolved using a mixed solution of HF + HNO_3 +- $HClO_4$ at ~150 °C for 10 days. The digested samples were evaporated and re-dissolved twice using 6 M (mol/L) HCl at ~100 °C, followed by dissolution in a 2.5 M HCl. Purification of Sr and Nd involves the classic two-step chromatography technique (Weis et al., 2006; Li et al., 2012). The first step was the separation of Sr and REE, in turn, from matrix elements using Bio-Rad AG50W-X12 resin (38–75 μm) by 5.0 M HCl and 6.0 M HCl, respectively. The second step involved the separation of Nd from REE fractions using HEHEHP resin (38–75 μm) by 0.2 M HCl. The total blanks were <200 pg for Sr and <100 pg for Nd. The mass fractionations of Sr and Nd isotopic ratios were corrected to $^{88}Sr/^{86}Sr = 8.375209$ and $^{146}Nd/^{144}Nd = 0.7219$, respectively. International reference materials of NBS-987 and JNdi-1 were determined to be 0.710250 ± 7 (2 SE) for $^{87}Sr/^{86}Sr$ and 0.512104 ± 5 (2 SE) for $^{143}Nd/^{144}Nd$. A USGS reference standard BCR-2 processed through the same analytical procedures yielded 0.705016 ± 10 (2 SE) for $^{87}Sr/^{86}Sr$ and 0.512623 ± 4 (2 SE) for $^{143}Nd/^{144}Nd$. All analyzed isotopic values of three reference standards match well with published data (e.g., Weis et al., 2006; Li et al., 2012).

3.2. Chemical analyses of magnetite

Major and trace element concentrations of magnetite were analyzed on polished thin sections (~50 μm in thickness) at the laboratory of Mineralization and Dynamics, Chang'an University (Luan et al., 2021), using a Photo Machines Analyte Excite 193 nm laser ablation system coupled with an Agilent 7700X quadrupole Inductively Coupled Plasma Mass Spectrometry (ICP-MS). The operating conditions were as follows: beam diameter of 65 μm, pulse rate of 5 Hz, beam fluence of 5.9 J/cm^2, and acquisition time of 15–20 s blank measurement (laser off) plus 40 s analysis (laser on). An international reference standard NIST610 was measured repetitively for every 8–10 analyses to monitor sensitivity drift.

Off-line raw data selection, integration of background and analysis signals, time-drift correction, quantitative calibration were conducted using the program ICPMSDataCal 7.2 (Liu et al., 2008). Multiple reference materials GSE-1G, BCR-2G, BIR-1G, and BHVO-2G were used as external standards for data calibration without applying an internal standard (Liu et al., 2008; Luan et al., 2021),

as magnetite contains abundant exsolution lamellae (Chen et al., 2014, 2017). During data reduction, the $Fe^{2+}/\Sigma Fe$ ratio of magnetite was set to be a value within the range of 0.35–0.48, which was analogical to the chemical compositions of magnetite obtained by electron probe microanalyzer (EPMA). Finally, the sum of all metal oxides was normalized to 100 wt% using Fe as the normalizing element (Liu et al., 2008). An in-house reference material BC-28 (massive magnetite collected from the Bushveld Complex, Dare et al., 2012) was determined for monitoring the data quality. The analytical result and detection limit of BC-28 are reported in Table S1, in agreement with previous studies (Fig. S3).

3.3. Magnesium isotope analyses

Magnesium isotopic analyses of magnetite were carried out at the Isotope Laboratory of the University of Washington, Seattle, following the procedures described in Sedaghatpour et al. (2013) and Chen et al. (2018). Briefly, magnetite separates were dissolved in concentrated HNO_3–HCl and then concentrated HCl. Sample solutions were passed through two steps of ion-exchange chromatography using (1) Bio-Rad AG1-X8 resin (38–75 μm) to eliminate Ti, and (2) Bio-Rad AG50W-X8 resin (38–75 μm) to separate Mg from other matrix elements. The purified Mg solutions were analyzed by a Nu II MC–ICPMS in a low-resolution mode using the standard-sample bracketing method (Teng and Yang, 2014). The analytical results were reported as $\delta^{X}Mg$ (‰) = $[(^{X}Mg/^{24}Mg)_{sample}/(^{X}Mg/^{24}Mg)_{DSM3} - 1] \times 1000$, where X refers to mass 25 or 26. The analytical precision, on the basis of multiple analyses ($n \geq 20$) of standards during an analytical session, was estimated to be better than ±0.07‰ (2 SD) for $\delta^{26}Mg$ and was compatible with the long-term external reproducibility (Teng et al., 2015). Four reference materials (DTS-1, PCC-1, San Carlos olivine, and Hawaiian seawater) were processed through the same procedures of column chemistry and instrumental measurement to evaluate the data accuracy and yielded similar values to literature data (Table S2).

4. RESULTS

Results are presented in Table 1 for Mg isotopic compositions of magnetite, Table S3 for whole-rock major element and Sr–Nd isotope compositions, and Table S4 for major and trace element compositions of magnetite. Whole-rock major element concentration, MgO concentration in magnetite, and Mg isotopic compositions of magnetite (together with ilmenite and silicates) along the stratigraphic section of the Baima intrusion are illustrated in Fig. 2.

4.1. Whole-rock major element and Sr–Nd isotope geochemistry

The cumulate rocks of the Baima intrusion display large ranges of major element compositions, with 12.8–46.6 wt% SiO_2, 2.85–14.7 wt% MgO, 10.7–58.0 wt% $Fe_2O_{3(T)}$, and 1.76–10.4 wt% TiO_2 (Table S2). Specifically, the oxide-rich rocks contain higher contents of $Fe_2O_{3(T)}$ (33.5–58.0 wt% vs. 10.7–24.9 wt%) and TiO_2 (4.93–10.4 wt% vs. 1.66–8.09 wt%) than the oxide-barren ones. By contrast, the former has lower MgO and SiO_2 contents than the latter (Fig. 2).

Initial Sr–Nd isotopic compositions are calculated to the emplacement age of the Baima intrusion at ~260 Ma (Zhou et al., 2008). The $(^{87}Sr/^{86}Sr)_i$ and $\varepsilon_{Nd}(t)$ of the oxide-rich rocks vary from 0.70488 to 0.70495 and from +1.3 to +3.5, respectively. The $(^{87}Sr/^{86}Sr)_i$ and $\varepsilon_{Nd}(t)$ of the oxide-barren rocks are similar to those of the oxide-rich ones, ranging from 0.70493 to 0.70512 and from +1.0 to +2.7, respectively (Table S3). These values are consistent with the published $(^{87}Sr/^{86}Sr)_i$ and $\varepsilon_{Nd}(t)$ of the Baima intrusion (0.70487–0.70520 and +0.6 to +4.6, respectively; Zhou et al., 2008; Yu et al., 2015).

4.2. Major and trace element compositions of magnetite

Major element contents of magnetite are highly variable in different lithofacies (Table S4). Magnetite crystals in the oxide-rich rocks are rich in MgO (0.81–1.63 wt%) (Fig. 2) and TiO_2 (8.04–14.8 wt%). By contrast, magnetite crystals in the oxide-barren rocks are relatively depleted in MgO (0.37–0.99 wt%) (Fig. 2) and TiO_2 (2.84–10.6 wt%). The MgO is positively correlated with TiO_2 in magnetite (Fig. 3a). Besides, most magnetite rims to which adjoin olivine and clinopyroxene have lower MgO contents than their cores (Fig. 4).

Trace element contents of magnetite are highly variable in different lithofacies as well (Table S4). Magnetite crystals in the oxide-rich rocks have higher concentration of compatible trace elements (e.g., Ni = 77.1–447 ppm, Co = 82.2–165 ppm, and Sc = 6.10–14.6 ppm) than those of the oxide-barren rocks (e.g., Ni = 13.6–128 ppm, Co = 61.5–155 ppm, and Sc = 1.36–8.52 ppm). Except for a few samples, magnetite grains display positive correlations between Ni and Co and Sc (Fig. 3b and c). On the other hand, magnetite grains in the oxide-rich rocks have comparable concentration of incompatible trace elements, such as Zr, to those of the oxide-barren rocks.

4.3. Magnesium isotope compositions of magnetite

Some magnetite grains may contain tiny exsolution lamellae (e.g., ilmenite and/or spinel), nonetheless, all of them were digested. Thus, the analytical results are the initial Mg isotope compositions of magnetite prior to subsolidus exsolution. Overall, $\delta^{26}Mg$ values in magnetite vary from -0.18 ± 0.06 to $+0.98 \pm 0.04$‰ (Fig. 2). Specifically, magnetite separates from the oxide-rich rocks have $\delta^{26}Mg$ ranging from -0.17 ± 0.06 to $+0.58 \pm 0.04$‰, with an average of +0.13‰. Those from the oxide-barren rocks have $\delta^{26}Mg$ varying from -0.18 ± 0.06 to $+0.98 \pm 0.04$‰, with an average of +0.36‰. Magnetite is isotopically heavier than most of the coexisting olivine ($\delta^{26}Mg$ = -0.33 to +0.05‰) and clinopyroxene (−0.29 to −0.13‰) (Chen et al., 2018) as well as the picritic and basaltic lavas in the Emeishan large igneous province (−0.36 to −0.19‰, Tian et al., 2017; Yu et al., 2020), the mantle (-0.25 ± 0.04‰, Teng et al., 2010), and global MORBs (-0.25 ± 0.06‰, Teng, 2017).

Table 1
Magnesium isotopic compositions (per mil) of magnetite and ilmenite separates from the Baima intrusion and its country rocks.

Zone	Height from the base (m)	Rock type	Sample No.	$\delta^{26}Mg_{magnetite}$	2 SD	$\delta^{25}Mg_{magnetite}$	2 SD	$\delta^{26}Mg_{ilmenite}$	2 SD	$\delta^{25}Mg_{ilmenite}$	2 SD	$\Delta^{26}Mg_{magnetite\text{-}ilmenite}$
	1014	Apatite-gabbro	SB11-52	0.07	0.06	0.06	0.03	0.24	0.06	0.13	0.05	−0.17
	950	Apatite-gabbro	SB11-81	0.13	0.06	0.08	0.04	1.03	0.05	0.52	0.04	−0.91
	839	Apatite-olivine-gabbro	SB11-69	0.39	0.06	0.23	0.05	1.57	0.05	0.81	0.04	−1.18
	820	Apatite-olivine-gabbro	SB11-68	0.43	0.06	0.22	0.05	1.21	0.05	0.63	0.04	−0.79
	798	Apatite-olivine-gabbro	SB11-56	0.70	0.06	0.39	0.03	1.21	0.04	0.61	0.03	−0.51
	775	Apatite-olivine-gabbro	SB11-57	0.30	0.06	0.18	0.03	1.10	0.05	0.52	0.04	−0.80
	760	Apatite-olivine-gabbro	SB11-64	−0.18	0.06	−0.08	0.04	0.39	0.05	0.21	0.04	−0.57
Upper Zone	720	Apatite-olivine-gabbro	SB11-100	−0.07	0.06	−0.03	0.05	0.09	0.05	0.05	0.04	−0.16
	680	Troctolite	**SB09-39**	**0.60**	**0.04**	**0.34**	**0.03**	0.02	0.05	0.03	0.04	0.57
			SB09-39*	0.54	0.05	0.31	0.04					
			SB09-39	0.68	0.06	0.37	0.04					
	575	Troctolite	SB09-37	0.22	0.06	0.12	0.04	0.28	0.04	0.14	0.03	−0.06
	540	Troctolite	**SB09-32**	**0.98**	**0.04**	**0.49**	**0.03**	1.28	0.06	0.64	0.05	−0.31
			SB09-32*	0.97	0.05	0.49	0.04					
			SB09-32	0.99	0.05	0.49	0.04					
	495	Troctolite	SB09-31	0.78	0.06	0.42	0.03	1.90	0.06	0.95	0.05	−1.12
	415	Olivine-gabbro	SB09-29	0.68	0.06	0.36	0.03	1.63	0.06	0.83	0.05	−0.95
Middle Zone	385	Olivine-gabbro	SB09-28	0.52	0.06	0.26	0.03	1.11	0.03	0.57	0.03	−0.59
	355	Magnetite-troctolite	SB09-27	−0.02	0.06	−0.01	0.04	0.35	0.04	0.19	0.04	−0.37
	325	Magnetite-troctolite	SB09-25	0.02	0.06	−0.01	0.04	−0.22	0.04	−0.12	0.03	0.24
	295	Olivine-gabbro	SB09-24	−0.14	0.06	−0.07	0.04	1.51	0.04	0.78	0.03	−1.65
	266	Olivine-gabbro	SB09-20	0.32	0.06	0.17	0.04	−0.20	0.05	−0.08	0.04	0.52
	216	Magnetite-troctolite	SB09-19	0.18	0.06	0.09	0.04	−0.18	0.05	−0.09	0.04	0.36
	202	Magnetite-troctolite	SB09-18	0.08	0.06	0.03	0.04	−0.45	0.05	−0.23	0.04	0.53
	192	Magnetite-troctolite	SB09-17	0.30	0.06	0.13	0.04	−0.31	0.05	−0.14	0.04	0.61
	182	Magnetite-troctolite	SB09-16	−0.16	0.06	−0.07	0.04	0.89	0.05	0.45	0.04	−1.06
	157	Magnetite-wehrlite	**SB09-15**	**0.07**	**0.04**	**0.07**	**0.03**	−0.50	0.05	−0.26	0.04	0.57
			SB09-15*	0.03	0.05	0.04	0.04					
			SB09-15	0.13	0.06	0.09	0.04					
	137	Magnetite-troctolite	SB09-14	−0.17	0.06	−0.08	0.04					
	113	Magnetite-troctolite	SB09-13	0.29	0.06	0.16	0.04	−0.46	0.05	−0.23	0.04	0.74
	102	Magnetite-wehrlite	**SB09-11**	**0.58**	**0.04**	**0.32**	**0.03**	−0.35	0.04	−0.17	0.03	0.92
			SB09-11*	0.54	0.05	0.29	0.04					
			SB09-11	0.63	0.06	0.34	0.04					
Lower Zone	60	Magnetite-wehrlite	SB09-08	0.25	0.06	0.13	0.04	−0.08	0.05	−0.03	0.04	0.33
		Siliceous marble	SB11-213	−1.01	0.06	−0.52	0.05					
		Siliceous marble	SB11-230	−1.78	0.06	−0.92	0.05					
Country rock		Siliceous marble	SB11-231	−1.75	0.06	−0.90	0.05					

Mg isotopic compositions of ilmenite are from Chen et al. (2018).
2 SD refers to 2 times standard deviation of the population of n ($n > 20$) repeated analyses of the standards during an analytical session.
The average value and associated 2 SD (the boldface numbers) are calculated from error-weighted values.
Due to isotope heterogeneity of magnetite separates from the same rock, the replicated samples show variations beyond the stated instrumental uncertainty.
* Represents replicate samples, including repeated sample dissolutions, column chemistry, and instrumental measurements.

Magnetite displays variable Mg isotopic features in comparison with coexisting ilmenite (Fig. 2). Magnetite separates in the oxide-rich rocks are most isotopically heavier than ilmenite, with $\Delta^{26}Mg_{magnetite\text{-}ilmenite}$ ranging from +0.24 to +0.92‰ (Table 1). Magnetite separates in the oxide-barren rocks are predominantly lighter than ilmenite, with $\Delta^{26}Mg_{magnetite\text{-}ilmenite}$ ranging from −1.65 to −0.06‰ (Table 1). Both magnetite and ilmenite in the oxide-rich rocks display relatively smaller variations in $\delta^{26}Mg$ than those in the oxide-barren ones (Fig. 5).

The $\delta^{26}Mg$ values of magnetite exhibit two distinct trends against whole-rock chemical compositions. $\delta^{26}Mg$ is negatively correlated with SiO_2 (and CaO, not shown) and positively correlated with MgO, $Fe_2O_{3(T)}$, and TiO_2 in the oxide-rich rocks. Opposite trends are observed in the oxide-barren rocks (Fig. 5).

5. DISCUSSION

The formation of Fe–Ti oxides in the Baima intrusion may involve multiple magmatic processes (e.g., fractional crystallization, magma mixing, crustal assimilation, and trapped liquid shift) and subsolidus processes (e.g., compositional exchange among minerals during cooling) (Shellnutt and Pang, 2012; Zhang et al., 2012, 2013; Chen et al., 2014; Liu et al., 2014b). Both could potentially lead to large Mg isotopic variations in magnetite. Since the Fe–Ti oxides in the Baima intrusion are fresh (Fig. S2), post-magmatic hydrothermal alteration can be ruled out as the cause of Mg isotopic variation in magnetite, which is further supported by the lack of correlation between $\delta^{26}Mg$ of magnetite and loss-on-ignition (LOI) and Rb concentration of whole rocks (Fig. S4).

Below, we focus our discussions on the role of magmatic and subsolidus processes in Mg isotopic variation, followed by the petrogenetic implications.

5.1. Magmatic processes are not responsible for Mg isotope variation in magnetite

Fractionation of silicate minerals would not induce resolvable Mg isotope variation during magmatic differentiation, which is evidenced by the limited Mg isotopic variations in global MORBs and ocean island basalts (Teng et al., 2007, 2010). Fractionation of oxide minerals, such as chromite or ilmenite, might drive the evolved melt (and crystallizing minerals) toward either light or heavy Mg isotopes (Su et al., 2017, 2019; Chen et al., 2018). The extensive depletion of Cr in magnetite indicated that the parental magma of the Baima intrusion had undergone crystallization of chromite at depth (Zhang et al., 2012). However, both olivine and clinopyroxene in the Baima intrusion display relatively small variation in $\delta^{26}Mg$ (−0.33 to +0.05‰ and −0.29 to −0.13‰, respectively; Chen et al., 2018) when compared to magnetite, suggesting limited Mg isotopic variation in their parental magma. Petrological and geochemical studies indicated that magnetite most likely crystallized from the same parental magma as the coexisting silicates (Zhang et al., 2012; Chen et al., 2014). Thus, crystallization of chromite from the same parental magma cannot explain the large Mg isotopic variation in magnetite.

Another unlikely case is that different parental magmas were involved in the formation of these Fe–Ti oxides and coexisting olivine and clinopyroxene. Such hypothetical magmas might originate from magma replenishment, residual liquids after silicate crystallization and/or filter-pressing processes, and silicate liquid immiscibility. However, quantitative models suggest that the magnitude of $\delta^{26}Mg$ offset for evolved melts would be less than 0.10‰ during magmatic differentiation (Fig. 6), even though the mole fraction of MgO removed via fractionation of one mineral is up to 50%. Furthermore, the $\delta^{26}Mg$ values of magnetite are not correlated with concentrations of Ni, Sc, and Cr in magnetite (Fig. 7a–c), proxies of magmatic evolution for Fe–Ti oxide-bearing layered mafic intrusions (Chen et al., 2017; Dare et al., 2019), indicating that fractional crystallization from diverse mafic magmas can also be ruled out.

Magnesium isotopic compositions of mantle-derived magmas could also be modified by crustal assimilation during magmatic evolution (Brewer et al., 2018; Pang et al., 2020; Chen et al., 2021). Contributions of crustal rocks to the petrogenesis of layered mafic–ultramafic intrusions in the Emeishan large igneous province are still debated. Oxygen isotopic compositions of magnetite and plagioclase require ~8–13% assimilation of the carbonate footwall during the parental magma evolution of the Panzhihua intrusion (Ganino et al., 2008, 2013). Instead, integrated O-Sr-Nd studies suggested negligible assimilation of crustal rocks (Song et al., 2013; Yu et al., 2015). Nonetheless, the country rocks (e.g., siliceous marble) of the Baima intrusion have low $\delta^{26}Mg$ (−1.78 ± 0.06 to −1.01 ± 0.06‰; Table 1), low $\varepsilon_{Nd}(t)$ (−2.9 to −0.6), and high $(^{87}Sr/^{86}Sr)_i$ (0.70579–0.70783) (Yu et al., 2015). The lack of correlations between $\delta^{26}Mg$ of magnetite and whole-rock $(^{87}Sr/^{86}Sr)_i$ and $\varepsilon_{Nd}(t)$ in the Baima intrusion implies that the assimilation of crustal rocks cannot be responsible for Mg isotope variation in magnetite (Fig. 8).

The Fe–Ti oxides and silicate minerals would experience trapped liquid shift during cooling of magma chambers, i.e., early crystallized minerals re-equilibrate with interstitial liquid overprinting their original compositions (Barnes, 1986). However, this process would occur at relatively high temperatures (e.g., >900 °C) and crystals would re-equilibrate with trapped liquid, hence, the trapped liquid shift was expected to produce limited Mg isotopic variations in crystallized minerals. Moreover, there is no correlation between $\delta^{26}Mg$ values and concentration of Zr in magnetite (Fig. 7d), which is incompatible and is sensitive to trapped liquid effect during the formation of Fe–Ti oxide-bearing cumulate rocks (Chen et al., 2017; Dare et al., 2019). Therefore, the possibility of trapped liquid shift as the cause of Mg isotopic variations in magnetite can also be excluded.

5.2. Magnesium isotopic variations in Fe–Ti oxides during subsolidus processes

The distinct correlations between $\delta^{26}Mg$ of magnetite and whole-rock major element contents indicate that Mg

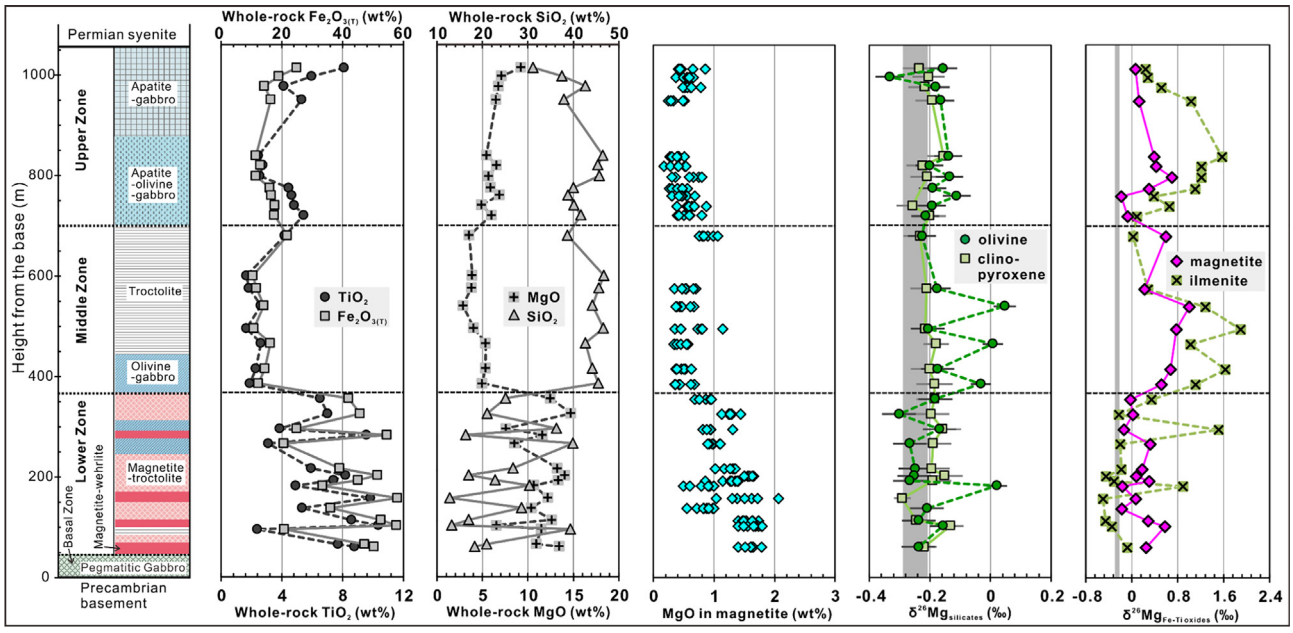

Fig. 2. Simplified stratigraphic columns of the Baima intrusion displaying the petrographic zones, MgO concentration in magnetite, major elemental variations of whole rocks, and Mg isotopic compositions of mineral separates. The petrographic zones are after Chen et al. (2014). MgO concentration of olivine and Mg isotopic compositions of olivine, clinopyroxene, and ilmenite are from Chen et al. (2018).

isotopic compositions of magnetite in the oxide-rich and oxide-barren rocks could be produced by different mechanisms during subsolidus processes, which is discussed in turn below.

5.2.1. Equilibrium fractionation between magnetite and ilmenite in oxide-rich rocks

Magnesium isotopic variation in magnetite in the oxide-rich rocks may result from equilibrium isotope fractionation between magnetite and ilmenite given the following consideration. Currently, no reduced partition function ratio (i.e., $10^3\ln\beta$) is available for magnetite. However, density functional perturbation theory (DFPT) calculations indicate that the temperature-dependent Mg isotope fractionations between spinel-structured phases and olivine are defined by (1) $\Delta^{26}Mg_{MgAl_2O_4-olivine} \approx +1.03 \times 10^6/T^2$, (2) $\Delta^{26}Mg_{MgCr_2O_4-olivine} \approx +0.33 \times 10^6/T^2$, and (3) $\Delta^{26}Mg_{MgFe_2O_4-olivine} \approx +0.23 \times 10^6/T^2$ (Schauble, 2011). Recent experimentally determined Mg isotope fractionations ($\Delta^{26}Mg_{MgAl_2O_4-olivine} \approx (+1.05 \pm 0.28) \times 10^6/T^2$ and $\Delta^{26}Mg_{MgCr_2O_4-olivine} \approx (+0.43 \pm 0.10) \times 10^6/T^2$) are consistent with those estimated by the DFPT calculations (Tang et al., 2021). Magnetite has the same inverse spinel structure as magnesioferrite ($MgFe_2O_4$). Additionally, magnetite has chemical components closer to magnesioferrite than spinel ($MgAl_2O_4$) and magnesiochromite ($MgCr_2O_4$). Hence, the $10^3\ln\beta$ of magnetite may resemble that of magnesioferrite and may be lower than those of spinel and magnesiochromite. The temperature-dependent Mg isotope fractionation between magnetite (assuming as same as magnesioferrite) and olivine is thus proposed to be $\Delta^{26}Mg_{magnetite\text{-}olivine} \approx +0.23 \times 10^6/T^2$. Besides, the $10^3\ln\beta$ of olivine and pyroxene are proposed to be higher than that of ilmenite, and the temperature-dependent isotope fractionation between olivine and ilmenite is $\Delta^{26}Mg_{olivne\text{-}ilmenite} \approx +0.27 \times 10^6/T^2$ (Chen et al., 2018). Therefore, the equilibrium Mg isotope fractionation between magnetite and ilmenite can be described by $\Delta^{26}Mg_{magnetite\text{-}ilmenite} \approx +0.50 \times 10^6/T^2$.

Most magnetite separates from the oxide-rich rocks are isotopically heavier than the coexisting ilmenite with $\Delta^{26}Mg_{magnetite\text{-}ilmenite}$ ranging from +0.24 to +0.92‰ (except two samples, Fig. 9a). These separates are also isotopically heavier than the coexisting olivine and clinopyroxene, with $\Delta^{26}Mg_{magnetite\text{-}olivine}$ and $\Delta^{26}Mg_{magnetite\text{-}clinopyroxene}$ ranging from +0.04 to +0.57‰ and from +0.16 to +0.53‰ (Fig. 9b and c), respectively. The direction of Mg isotope fractionation between magnetite and ilmenite is consistent with equilibrium isotope fractionation. However, the magnitude of the inter-mineral fractionation is too large to produce at magmatic temperatures (e.g., 950–1200 °C, Zhang et al., 2012) (Fig. 9a), and indicates isotope fractionations at lower temperature and during subsolidus processes.

Magnetite grains are predominantly adjacent to each other and/or ilmenite in oxide-rich rocks at Baima (Fig. S2). The coexisting magnetite and ilmenite would undergo extensive re-equilibration via the reaction: Mg^{2+} (in magnetite) + Fe^{2+} (in ilmenite) = Mg^{2+} (in ilmenite) + Fe^{2+} (in magnetite) (Lindsley, 1991). This reaction shifts to the right during cooling. The abundant exsolution lamellae of ilmenite in magnetite demonstrate significant subsolidus re-equilibration between Fe–Ti oxides (Zhang et al., 2012). Moreover, the blocking temperature of Mg^{2+} and Fe^{2+} re-equilibration between magnetite and ilmenite was estimated to be as low as

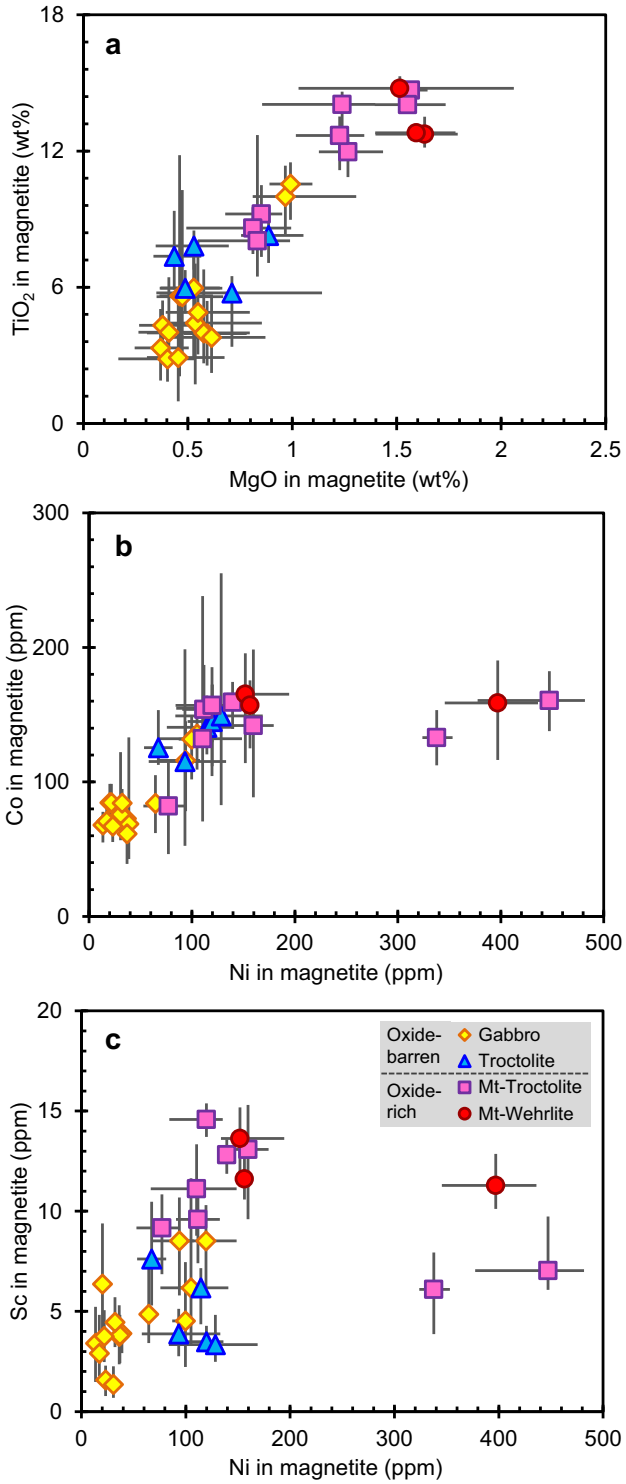

Fig. 3. Plots of (a) MgO vs. TiO_2, (b) Ni vs. Co, and (c) Ni vs. Sc in magnetite. Error bars represent the concentration ranges measured in this study. Mt-wehrlite and Mt-troctolite refer to magnetite-wehrlite and magnetite-troctolite, respectively. Data are from Table S4.

~500 °C, which was much lower than those between Fe-Ti oxides and silicates (i.e., ~950 °C) (Pang et al., 2008b; Chen et al., 2014; Liu et al., 2015). The observed $\Delta^{26}Mg_{magnetite\text{-}ilmenite}$ values in the oxide-rich rocks mostly fall within the range of equilibrium fractionations between ~500 and 950 °C (Fig. 9a). This result strongly supports that Mg isotopic compositions of magnetite in the oxide-rich rocks were primarily governed by equilibrium isotope fractionation between Fe–Ti oxides during sub-solidus re-equilibration.

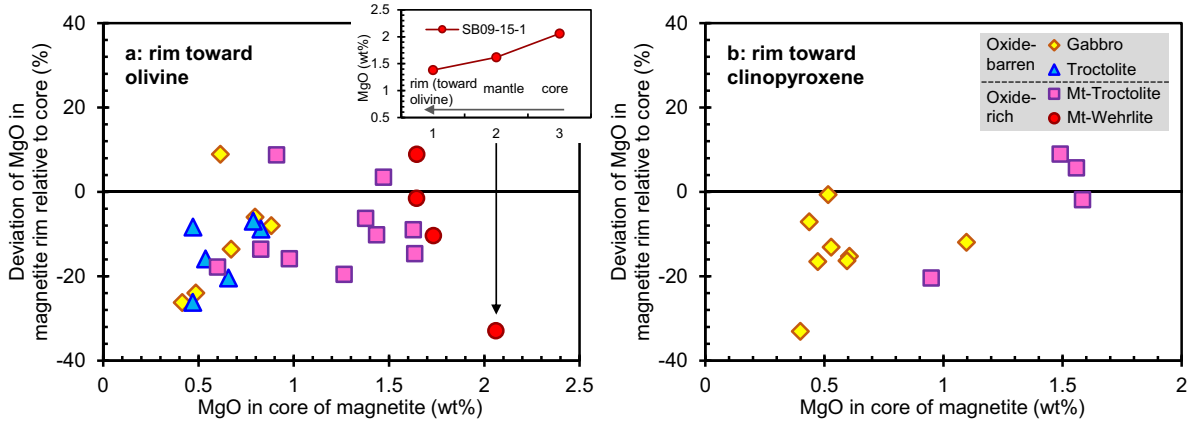

Fig. 4. Plots of deviation of MgO in magnetite rims relative to cores ((MgO_{rim} − MgO_{core})/MgO_{core}) × 100%) vs. MgO concentration in magnetite cores. Statistically, the magnetite rims next to olivine (a) and clinopyroxene (b) have lower MgO than the cores, particularly for those crystals in the oxide-barren rocks. The inserted figure shows the MgO profile of a magnetite from core to rim. Data are reported in Table S4.

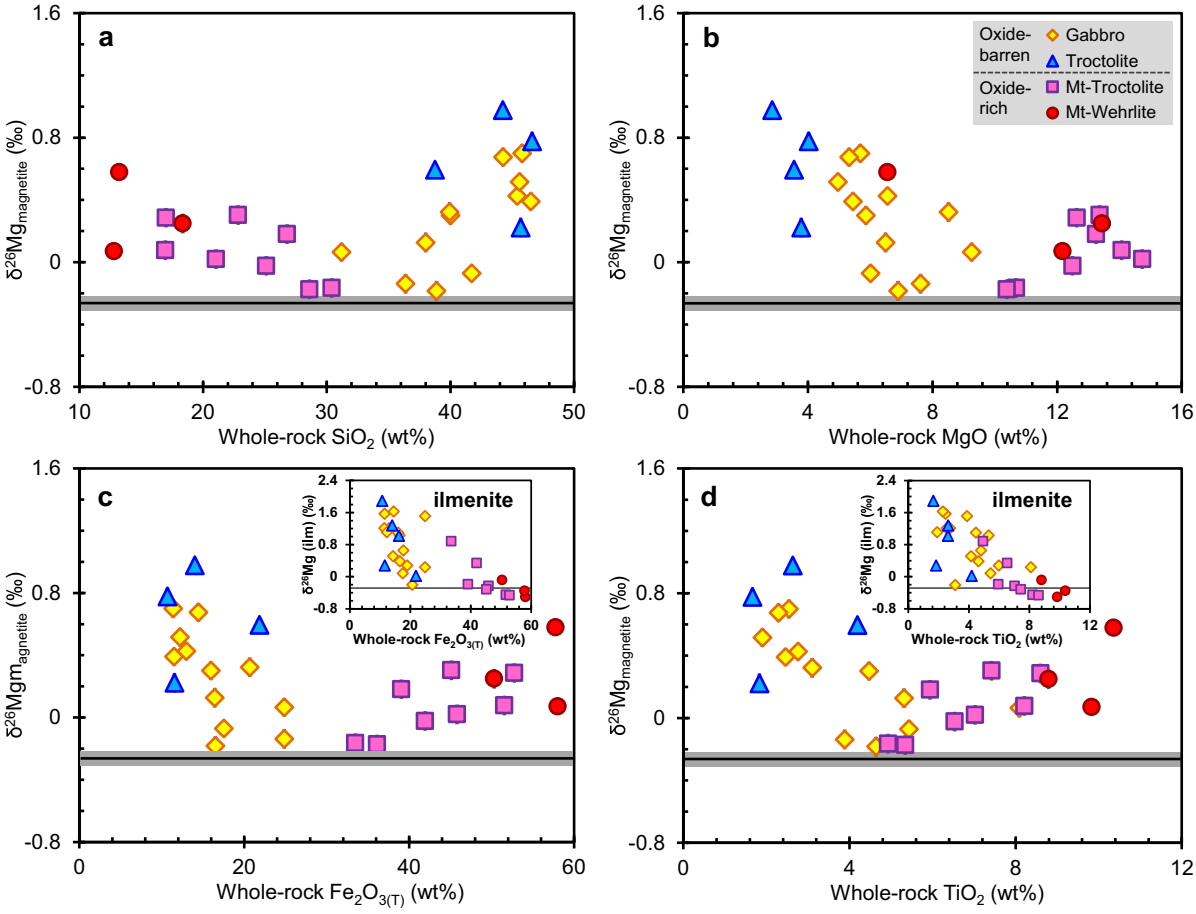

Fig. 5. Plots of $\delta^{26}Mg$ in magnetite vs. (a) SiO_2, (b) MgO, (c) $Fe_2O_{3(T)}$, and (d) TiO_2 of whole rocks. The inserted figures display $\delta^{26}Mg$ in ilmenites vs. $Fe_2O_{3(T)}$ and TiO_2 of whole rocks (Chen et al., 2018). Error bars of Mg isotopes for most samples are smaller than symbol sizes. The horizontal black line and gray bar represent the average Mg isotopic value of the mantle (−0.25 ± 0.04‰, Teng et al., 2010).

Since heavy isotopes of Mg and Fe are more enriched in magnetite than ilmenite, $\delta^{26}Mg$ would be expected to positively correlate with $\delta^{57}Fe$ in magnetite in the oxide-rich rocks during inter-oxide re-equilibration. However, a weakly negative correlation between $\delta^{26}Mg$ and $\delta^{57}Fe$ in magnetite in the oxide-rich rocks is observed

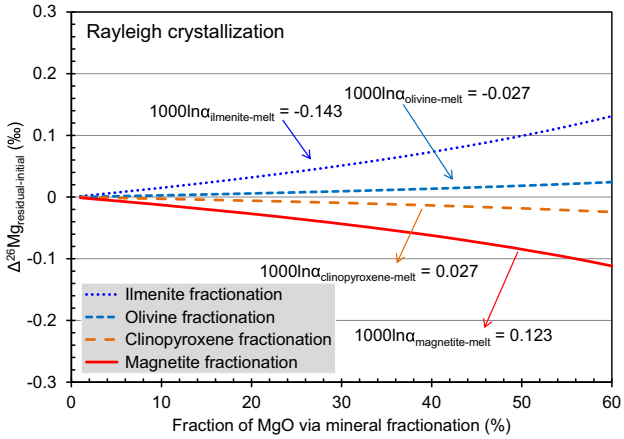

Fig. 6. Rayleigh fractionation model ($\delta^{26}Mg_{residual}/\delta^{26}Mg_{initial} = f^{\alpha-1}$) for Mg isotope fractionation during magmatic differentiation. The fractionation factor between olivine and silicate melt ($\alpha_{olivine\text{-}melt}$) is assumed as 0.99997, which falls within the range of 0.99993–1.00007 proposed by Teng et al. (2007). The fractionation factors between other minerals and silicate melt ($\alpha_{clinopyroxene\text{-}melt}$ = 1.00003, $\alpha_{ilmenite\text{-}melt}$ = 0.99986, and $\alpha_{magnetite\text{-}melt}$ = 1.00012) are estimated from Schauble (2011), Chen et al. (2018) and this study. The temperature is set to be 1100 °C in this model calculation. Model results show limited Mg isotope fractionation during magmatic differentiation.

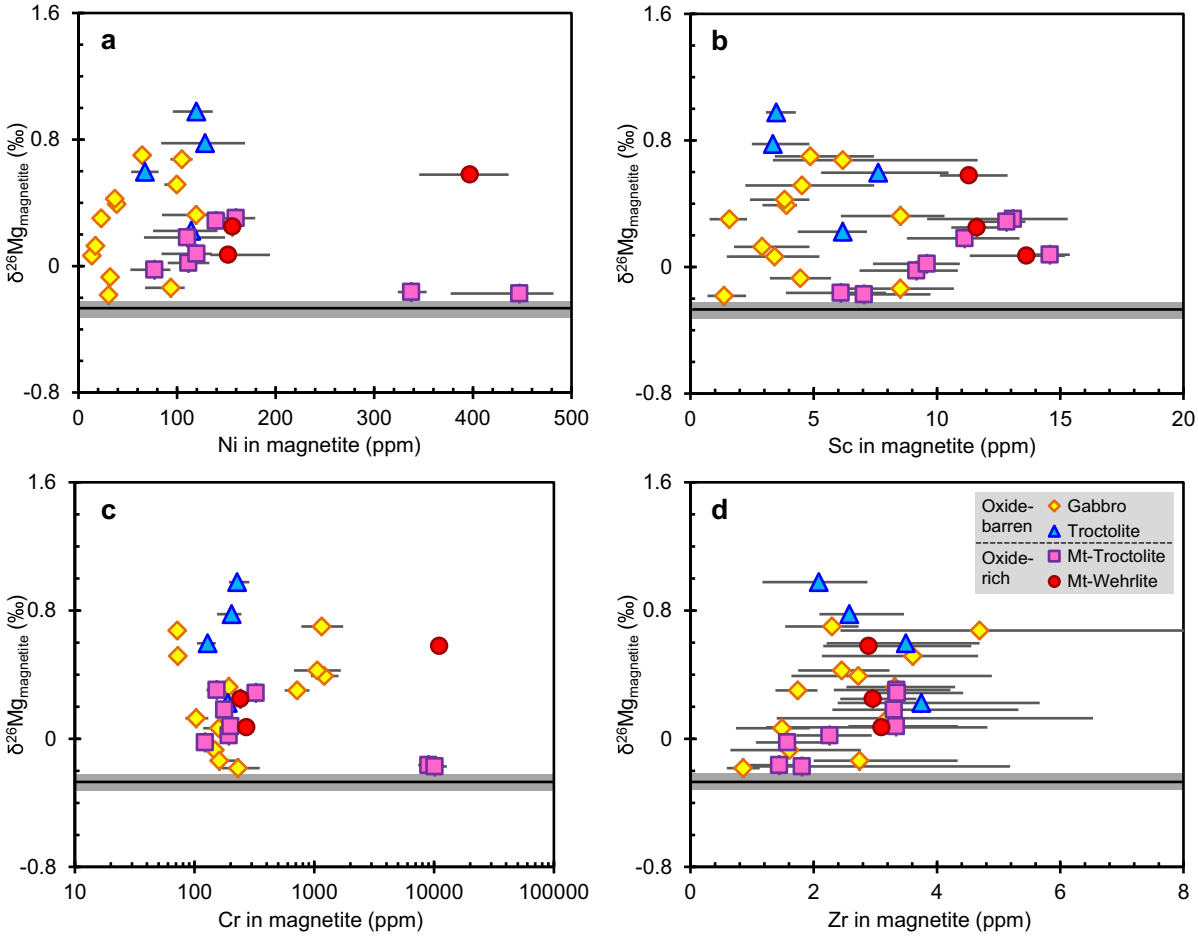

Fig. 7. Plots of $\delta^{26}Mg$ vs. (a) Cr, (b) Ni, (c) V, and (d) Zr concentrations in magnetite. Error bars represent the concentration ranges measured in this study. Data are from Tables 1 and S4.

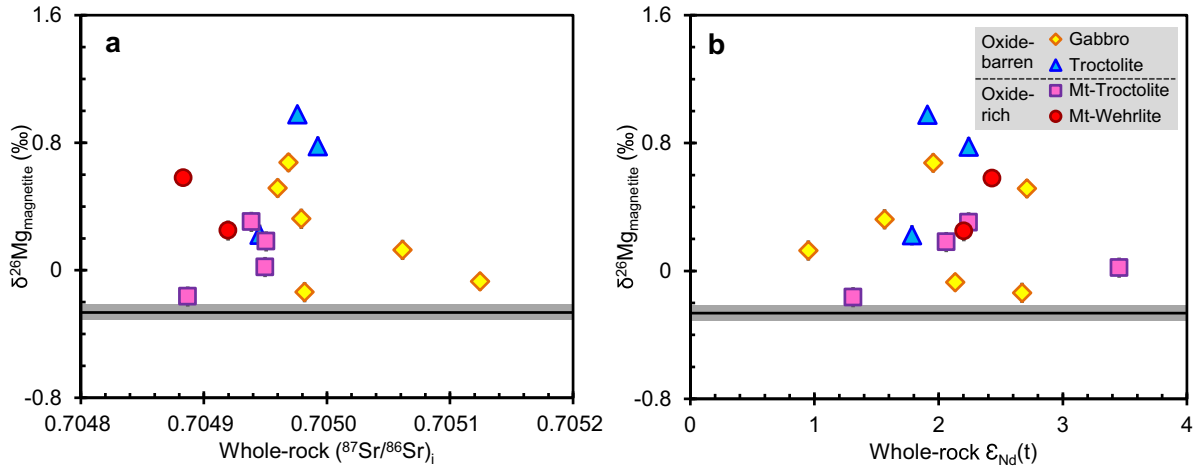

Fig. 8. Plots of $\delta^{26}Mg$ in magnetite vs. (a) $(^{87}Sr/^{86}Sr)_i$ and (b) $\varepsilon_{Nd}(t)$ in whole rocks. The initial Sr and Nd isotopic compositions were calculated to the emplacement age of ~260 Ma (Zhou et al., 2008).

(Fig. S5). This discrepancy may be due to the low concentration of MgO (<1.8 wt%) but high FeO_{Total} (~42–47 wt % Fe_2O_3 and ~35–40 wt% FeO) in magnetite. The $\delta^{26}Mg$ of magnetite is only controlled by Mg^{2+}, whereas $\delta^{57}Fe$ is determined by both Fe^{2+} and Fe^{3+}. Both fractional crystallization and subsolidus re-equilibration would generate different effects on Mg and Fe isotopic compositions, leading to the decoupled $\delta^{26}Mg$ and $\delta^{57}Fe$ in magnetite (Fig. S5).

5.2.2. Diffusion-driven kinetic Mg isotope fractionation in oxide-barren rocks

Most magnetite separates from the oxide-barren rocks are isotopically lighter than coexisting ilmenite, with $\Delta^{26}Mg_{magnetite\text{-}ilmenite}$ ranging from −1.65 to −0.06‰ (Fig. 9a). They are also much heavier than coexisting olivine and clinopyroxene, with $\Delta^{26}Mg_{magnetite\text{-}olivine}$ and $\Delta^{26}Mg_{magnetite\text{-}clinopyroxene}$ varying from +0.03 to +1.02‰ (except one sample) and from +0.02 to +0.99‰ (Fig. 9b and c), respectively. These results are opposite to the direction and/or magnitude of equilibrium isotope fractionation, hence most likely indicative of kinetic isotope fractionation driven by chemical diffusion between magnetite and ferromagnesian silicates. This hypothesis is strongly favored by (1) the low MgO concentration in magnetite (Fig. 3a and b) and (2) the negative correlation of $\delta^{26}Mg$ with MgO concentration in magnetite (Fig. 10).

Micro-textures and chemical compositions of coexisting minerals in mafic–ultramafic cumulates indicate that Mg^{2+} would diffuse from magnetite into ferromagnesian silicates as temperature decreases (Morse, 1980; Pang et al., 2008b). Indeed, MgO content in olivine decreases from ~37.0 to ~24.8 wt% upward in the Baima intrusion (Chen et al., 2018), while magnetite displays an extensive decrease of MgO from 1.63 to 0.37 wt% upward. The ratios of $MgO_{olivine}$ to $MgO_{magnetite}$ in the oxide-barren rocks (22.2–41.6, with an average of 29.2) are much lower than those of the oxide-rich ones (32.2–70.9, with an average of 53.7), both of which are lower than that of the experimental results (~7, Toplis and Carroll, 1995) (Fig. S6). Moreover, the Mg–Fe inter-diffusion coefficients ($D_{Mg\text{–}Fe}$) in olivine and clinopyroxene are at least two orders of magnitude lower than those of Mg^{2+} in Fe-Ti oxides (Chakraborty, 2010; Cherniak and Dimanov, 2010; Van Orman and Crispin, 2010). Thus, the blocking temperature of Mg^{2+} in ferromagnesian silicates is much higher than that in Fe-Ti oxides (Pang et al., 2008b; Chen et al., 2014). Most magnetite rims in contact with ferromagnesian silicates have slightly lower MgO concentration than their cores (Fig. 4). Correspondingly, olivine rims in contact with Fe–Ti oxides have higher Fo values (Fo = 100 × MgO/(FeO + MgO), in mole) than the inner zones (Fig. S7). All these observations imply the diffusion of Mg^{2+} from Fe–Ti oxides into ferromagnesian silicates during the cooling of the Baima magma chamber. Since light isotopes diffuse faster than heavy ones (Richter et al., 2008, 2009), diffusion of Mg^{2+} out of magnetite generated the observed high $\delta^{26}Mg$ of magnetite and large $\Delta^{26}Mg_{magnetite\text{-}olivine}$ and $\Delta^{26}Mg_{magnetite\text{-}clinopyroxene}$ values.

Diffusion-driven Mg isotope fractionation in magnetite can be quantitatively calculated using the equation presented in Zhu et al. (2015):

$$\Delta Mg_{High-Low}\ (‰) = 1000 \times [1 - (m_2/m_1)^{\beta})] \times (1 - C_{Low}/C_{High}) \quad (1)$$

where $\Delta Mg_{High\text{-}Low}$ is isotope fractionation between high and low concentration end-members; m_1 and m_2 represent masses of heavy and light isotopes, respectively; C_{High} and C_{Low} denote MgO contents in high and low concentration end-members, respectively; β is the empirical factor. This equation was derived from Fick's law of diffusion (Zhu et al., 2015) and is identical to the equation for modeling non-equilibrium isotope fractionation proposed by Watson and Müller (2009). Bulk element and isotope compositions of one crystal (C_{bulk} and δ_{bulk}, respectively) that is set as a sphere were quantitatively modeled using the following equations:

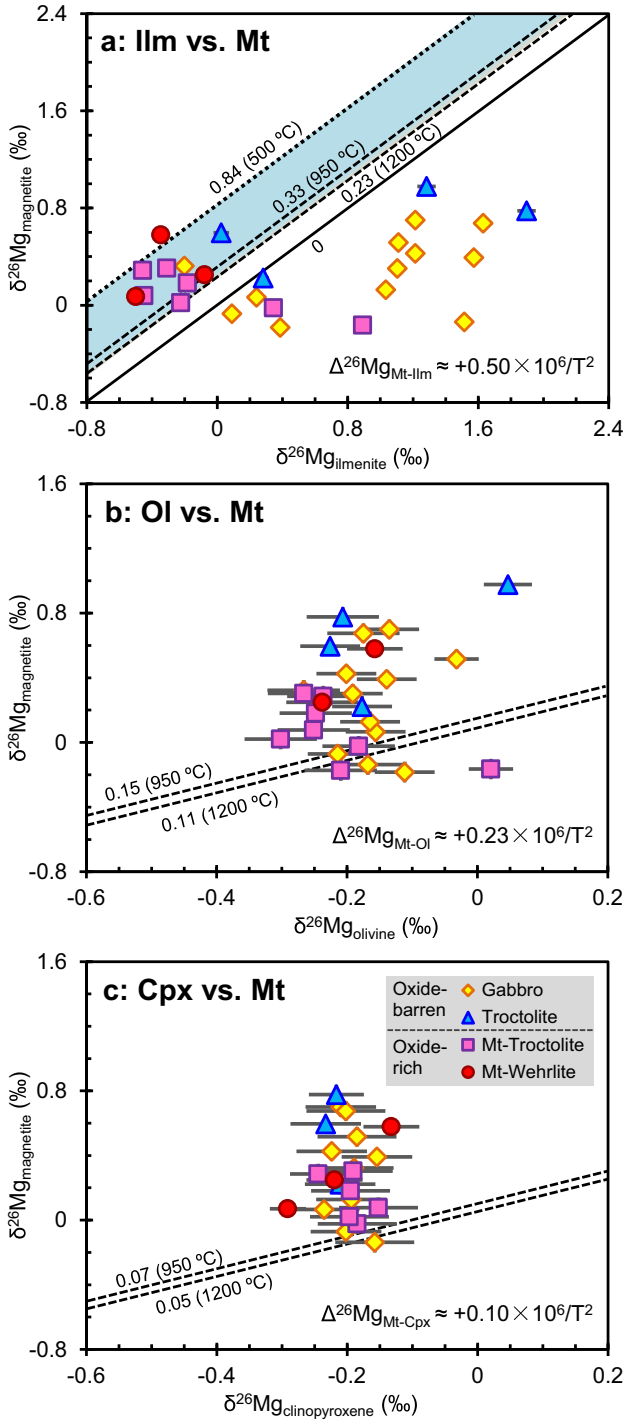

Fig. 9. Mg isotope fractionation (a) between magnetite and ilmenite, (b) between magnetite and olivine, and (c) between magnetite and clinopyroxene in the Baima intrusion. Magnesium isotopic compositions of olivine, clinopyroxene, and ilmenite are from Chen et al. (2018). The temperature-dependent equilibrium Mg isotope fractionations among minerals are estimated from Schauble (2011) and Chen et al. (2018). The dash lines mean equilibrium isotope fractionation at variable temperatures of magmatic processes (~950–1200 °C, Zhang et al., 2012) and subsolidus processes (~500 °C, Pang et al., 2008b; Liu et al., 2014a).

$$C_{bulk} = \int_0^R 4\pi C(r) r^2 dr \Big/ \int_0^R 4\pi r^2 dr \quad (2)$$

$$\delta_{bulk} = \int_0^R 4\pi \delta(r) C(r) r^2 dr \Big/ \int_0^R 4\pi C(r) r^2 dr \quad (3)$$

β factor is set to be 0.08, which is identical to that of ilmenite (Chen et al., 2018). The $\delta^{26}Mg$ of the low concentration end-member in magnetite is assumed as −0.15‰, which represents the magnetite in equilibrium with mantle-like basaltic magmas. The model calculation can reproduce the observed

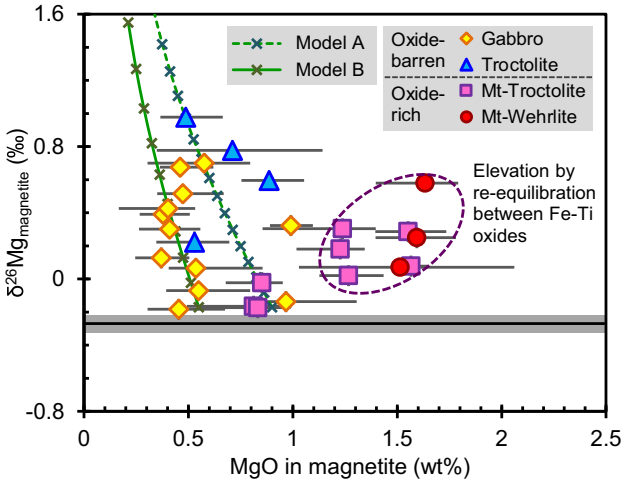

Fig. 10. Plot of δ^{26}Mg vs. MgO in magnetite. The initial MgO concentrations for models A and B are set to be 0.9 and 0.55 wt%, respectively. The ticks along the modeling curves (cross symbols) represent diffusion out of 0.05 wt% MgO from magnetite during subsolidus processes. Error bars for δ^{26}Mg are smaller than symbol sizes and error bars for MgO represent the concentration range measured in this study. The horizontal black line and gray bar mean the average Mg isotopic value of the mantle (-0.25 ± 0.04‰, Teng et al., 2010). See text for modeling details.

element and isotope compositions of most samples by assuming magnetite initially contained ~0.55–0.9 wt% MgO (Fig. 10). Our model also reveals that δ^{26}Mg of a mineral would increase rapidly after extensive loss of MgO by chemical diffusion (Fig. 10), which may provide an alternative explanation for the extremely high δ^{26}Mg of ilmenite in the Panzhihua intrusion (Tian et al., 2020).

A few magnetite separates from the oxide-barren rocks (e.g., SB09-24, SB11-64, and SB11-100) have relatively low δ^{26}Mg values, which may reflect the isotopic heterogeneity of magnetite grains. Although magnetite crystals are mainly in contact with silicates in the oxide-barren rocks (Fig. S2), they are adjacent to Fe-Ti oxides or isolated by plagioclase as well. If such magnetite grains were predominantly separated and analyzed, the observed δ^{26}Mg values would be relatively low due to equilibrium isotope fractionation between Fe–Ti oxides. Furthermore, subsolidus diffusion process is not expected to modify δ^{26}Mg values of coexisting ferromagnesian silicates due to their very high MgO concentration (>10 wt%) and modal abundances (>30%) in the oxide-barren rocks (Zhang et al., 2012; Chen et al., 2014). This hypothesis is supported by the similar Mg isotopic compositions of olivine and clinopyroxene in both oxide-rich and oxide-barren samples (Chen et al., 2018).

The overall Mg isotope variations in magnetite during magmatic and subsolidus processes are illustrated in Fig. 11. Magnetite crystallized from late-stage magma would have a δ^{26}Mg value of ~-0.15‰ as equilibrium isotope fractionation is expected between magnetite and magma (Fig. 11a). During cooling, magnetite may undergo three end-member elemental exchange processes depending on the coexisting minerals. In the scenario I, magnetite surrounded by other magnetites or isolated by plagioclase should preserve its initial Mg isotopic signature, with δ^{26}Mg of ~-0.15‰ (Fig. 11b). In the scenario II, magnetite adjacent to ilmenite should experience subsolidus re-equilibration with ilmenite, which led to the moderately heavy Mg isotopic compositions of magnetites, with δ^{26}Mg up to ~+0.55‰ (Fig. 11b). In the scenario III, magnetite in contact with ferromagnesian silicates underwent subsolidus chemical diffusion, which produced the extremely heavy magnetite, with δ^{26}Mg up to ~+1.0‰ (Fig. 11b). Therefore, a combination of these different scenarios would generate the heterogeneous Mg isotopic variation in magnetite (and ilmenite) in the Baima layered mafic intrusion.

5.3. Implication for origins of Fe–Ti oxides in layered mafic intrusions

Understanding the mechanisms for saturation and enrichment of Fe–Ti oxides during mafic magma evolution is of fundamental importance for igneous petrology (Wager and Brown, 1967; Veksler and Charlier, 2015). Such an issue, in particular, is prominent for the Fe–Ti oxides in layered mafic intrusions in the Emeishan large igneous province, as the thick Fe–Ti oxide horizons mainly occur in the lower and/or middle zones of these intrusions rather than in upper zones of other global layered mafic intrusions, such as the Bushveld Complex (e.g., Zhou et al., 2005, 2013; Song et al., 2013; Charlier et al., 2015). Two fundamental models have been proposed as the saturation and accumulation of magnetite and ilmenite in these intrusions. One is that the Fe-Ti oxides were late-stage crystallization from immiscible Fe-rich/oxide melts (e.g., Zhou et al., 2005, 2013; Wang and Zhou, 2013; Liu et al., 2014b; Wang et al., 2018). Another argues that they co-crystallized with silicate minerals from (ferro-)basaltic magmas (e.g., Pang et al., 2008a, 2008b; Zhang et al., 2012; Song et al., 2013; Howarth and Prevec, 2013; Bai et al., 2014; Chen et al., 2017). More recently, a few studies

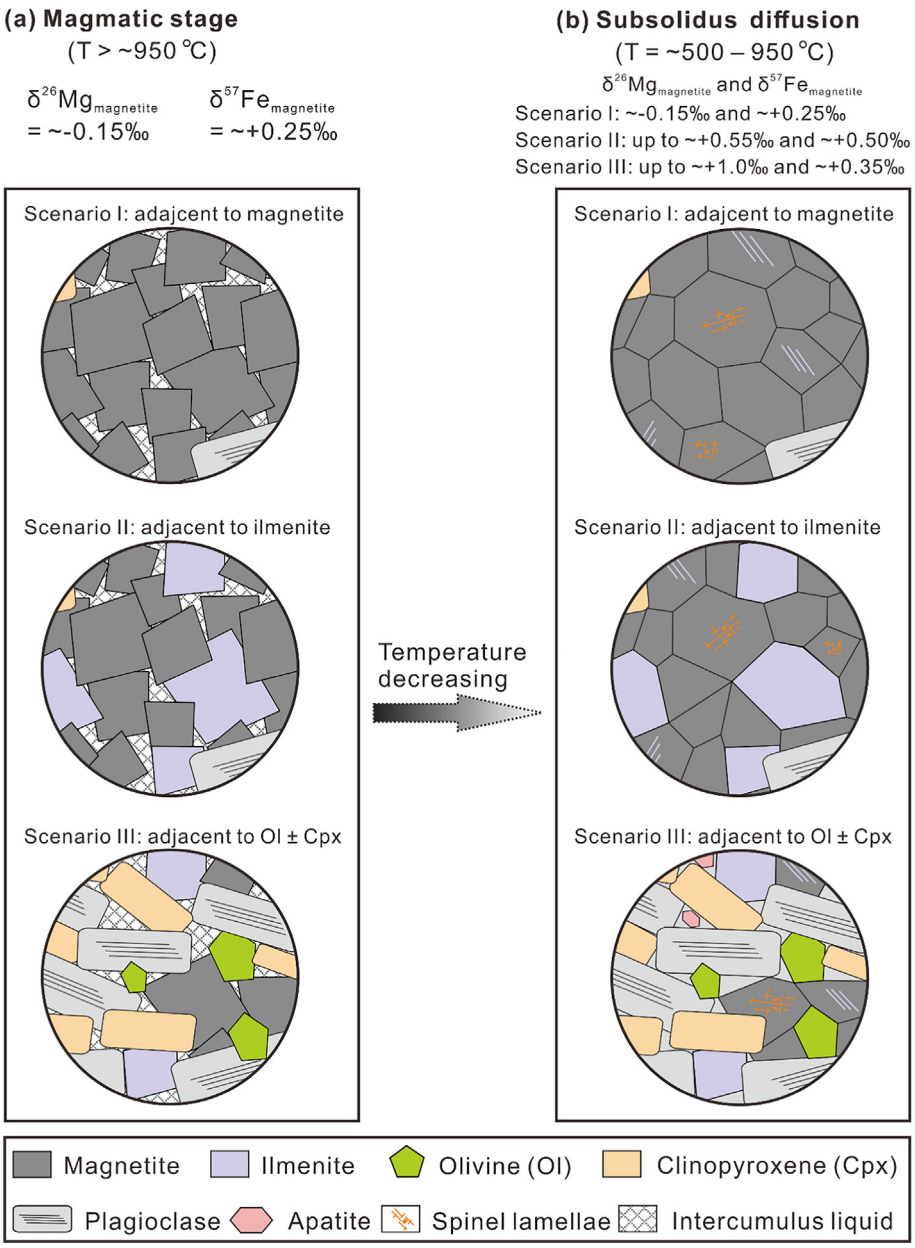

Fig. 11. Cartoon illustrating Mg isotope variation in magnetite (a) at the magmatic stage and (b) during subsolidus diffusion. Magnetite surrounded by other magnetites (scenario I) could preserve the initial Mg isotopic signature. Magnetite adjacent to ilmenite (scenario II) would experience subsolidus re-equilibration with ilmenite, which generated moderately heavy magnetite. Magnetite in contact with ferromagnesian silicates (scenario III) may undergo subsolidus chemical diffusion, which produced much heavy magnetite. The variations of Fe isotopic compositions in magnetite are based on Chen et al. (2014). See text for details.

inferred that the large variations of Mg isotopes in ilmenite and Fe isotopes in Fe–Ti oxides from the Panzhihua intrusion might support the genetic model of liquid immiscibility of Fe-rich melts during magmatic evolution (Cao et al., 2019; Tian et al., 2020).

The large Mg isotopic variations in magnetite and ilmenite from the Baima intrusion in this study are not consistent with the model of immiscible Fe-rich/oxide melts. Experimental studies show the partition coefficient of Mg^{2+} between Fe- and Si-rich melts ranging from ~2 to 3 (Schmidt et al., 2006; Veksler et al., 2006; Charlier and Grove, 2012). This partition coefficient is inconsistent with the hypothetical model of liquid immiscibility proposed by Tian et al. (2020), where the partition coefficient was assumed close to ~zero in order to generate the extremely low MgO (~0.001 wt%) in the hypothetical Si-rich melt. In addition, theoretical calculation suggests that light isotopes of Mg and Fe prefer Fe-rich melts to Si-rich melts during silicate liquid immiscibility (Zhu et al., 2015). Thus, the hypothetical Fe-rich melts proposed by Cao et al. (2019) would be enriched in light Mg isotopes if silicate liquid immiscibility had occurred during magma evolution. The fact that both

magnetite and ilmenite are isotopically heavy in the oxide-barren rocks is opposite to such an expectation, indicating that Fe–Ti oxides in layered mafic intrusions cannot be originated from immiscible Fe-rich/oxide melts.

Our results support the genesis of Fe–Ti oxides from early fractional crystallization of ferro-basaltic magmas. Although Mg isotope signatures of magnetite separates have been mostly elevated by subsolidus processes, those (SB09-14 and SB09-16) least affected have the most primitive δ^{26}Mg (-0.17 ± 0.06 to -0.16 ± 0.06‰), which are close to isotope equilibrium with olivine and clinopyroxene at magmatic temperatures (Figs. 9 and 10). Particularly, the parental magma of the Baima intrusion was genetically associated with high-Ti basalts in the Emeishan large igneous province (Zhou et al., 2008; Zhang et al., 2012), which had mantle-like δ^{26}Mg values (-0.25 ± 0.09‰) (Tian et al., 2017). Magnetite would have an Mg isotopic ratio of −0.14‰ (±0.09‰) at a temperature of ~1100 °C, assuming that equilibrium isotope fractionation between magnetite and magma is identical to that between magnetite and olivine. The most primitive Mg isotopic compositions of magnetite agree well with theoretically calculated equilibrium fractionation, implying that magnetite co-crystallized early with olivine during magmatic differentiation. These results are also consistent with the observation of equilibrium Fe isotope fractionation between magnetite and olivine in the oxide-rich rocks at Baima (Chen et al., 2014).

Our study also challenges the long-standing view that thermodynamic equilibrium has been reached in mafic–ultramafic rocks. Minerals in layered mafic intrusions have been commonly used to infer the nature of their parental magmas and magmatic evolution. Therefore, magnetite and ilmenite, as two widespread cumulus and intercumulus minerals, were utilized to constrain the origins of layered mafic intrusions (Jang et al., 2001; Jang and Naslund, 2003; Zheng et al., 2014). However, our studies found large chemical and isotopic disequilibrium in magnetite and coexisting minerals. Inter-mineral Mg, Fe, and Cr isotope disequilibrium fractionation also occurs in the Stillwater Complex, USA (Bai et al., 2019, 2021). The widespread preservation of disequilibrium among minerals in mafic–ultramafic cumulates may complicate the use of minerals to trace their parental magmas. Instead, it may help to characterize the petrogenesis and metallogenesis of mafic–ultramafic rocks.

6. CONCLUSIONS

Magnetite separates from the oxide-rich rocks in the Baima intrusion have δ^{26}Mg of -0.17 ± 0.06 to $+0.58 \pm 0.04$‰, which mainly resulted from equilibrium isotope fractionation produced by Mg–Fe re-equilibration between Fe–Ti oxides during subsolidus processes. By contrast, magnetite separates from the oxide-barren rocks have δ^{26}Mg ranging from -0.18 ± 0.06 to $+0.98 \pm 0.04$‰, which were ascribed to kinetic isotope fractionation driven by Mg–Fe inter-diffusion between magnetite and ferromagnesian silicates during subsolidus processes. The assemblage and modal abundance of coexisting minerals to which Fe–Ti oxides adjoin primarily controlled Mg isotopic variation in magnetite in layered mafic intrusions. These results provide significant insights into the behavior of Mg isotopes during high-temperature magmatic processes.

Our findings yield two significant implications. The most primitive Mg isotopic compositions of magnetite match well with theoretical equilibrium fractionation values, indicating that fractional crystallization played a major role in the genesis of Fe–Ti oxides in layered mafic intrusions. The widespread preservation of kinetic Mg isotope fractionation in magnetite suggests extensive compositional disequilibrium in mafic–ultramafic cumulates. Such disequilibrium effects indicate that subsolidus diffusion is an important process to characterize the petrogenesis and metallogenesis of mafic–ultramafic rocks.

Declaration of Competing Interest

The authors declare that they have no known competing financial interests or personal relationships that could have appeared to influence the work reported in this paper.

ACKNOWLEDGEMENTS

This study is jointly funded by the Strategic Priority Research Program (B) of the Chinese Academy of Sciences (XDB41020102 and XDB18000000), the NSFC (41873026 and 41473024), and the National Key R & D Program of China (2016YFC0600503). We are grateful to Drs. Yang Sun, Jin-Long Ma, Yan Hu, and Zhi-Hui Dai for their help on Mg isotopic and chemical analyses. We appreciate Dr. Val Finlayson and two anonymous reviewers for their insightful comments, which contribute greatly to the improvement of the manuscript. Drs. Shichun Huang (Associate Editor) and Jeffrey Catalano (Executive Editor) are acknowledged for their suggestions and editorial guidance. Prof. Dan Zhu and Mr. Jia-Fei Zhang are thanked for their assistance in modeling the diffusion effect and the fieldwork, respectively.

APPENDIX A. SUPPLEMENTARY MATERIAL

Supplementary data to this article can be found online at https://doi.org/10.1016/j.gca.2021.06.016.

REFERENCES

Bai Y., Su B.-X., Xiao Y., Chen C., Cui M.-M., He X.-Q., Qin L.-P. and Charlier B. (2019) Diffusion-driven chromium isotope fractionation in ultramafic cumulate minerals: Elemental and isotopic evidence from the Stillwater Complex. *Geochim. Cosmochim. Acta* **263**, 167–181.

Bai Y., Su B.-X., Xiao Y., Cui M.-M. and Charlier B. (2021) Magnesium and iron isotopic evidence of inter-mineral diffusion in ultramafic cumulates of the Peridotite Zone, Stillwater Complex. *Geochim. Cosmochim. Acta* **292**, 152–169.

Bai Z.-J., Zhong H., Li C., Zhu W.-G., He D.-F. and Qi L. (2014) Contrasting parental magma compositions for the Hongge and Panzhihua magmatic Fe-Ti-V oxide deposits, Emeishan large igneous province, SW China. *Econ. Geol.* **109**, 1763–1785.

Barnes S. (1986) The effect of trapped liquid crystallization on cumulus mineral compositions in layered intrusions. *Contrib. Mineral. Petr.* **93**, 524–531.

Bilenker L. D., VanTongeren J. A., Lundstrom C. C. and Simon A. C. (2017) Iron isotopic evolution during fractional crystallization of the uppermost Bushveld Complex layered mafic intrusion. *Geochem. Geophys. Geosyst.* **18**, 956–972.

Brewer A. W., Teng F.-Z. and Mullen E. (2018) Magnesium isotopes as a tracer of crustal materials in volcanic arc magmas in the northern Cascade Arc. *Front. Earth Sci.* **6**.

Cao Y., Wang C. Y., Huang F. and Zhang Z. (2019) Iron isotope systematics of the Panzhihua mafic layered intrusion associated with giant Fe-Ti oxide deposit in the Emeishan large igneous province, SW China. *J. Geophys. Res.-Sol. Earth* **124**, 358–375.

Chakraborty S. (2010) Diffusion Coefficients in Olivine, Wadsleyite and Ringwoodite. *Rev. Mineral. Geochem.* **72**, 603–639.

Charlier B. and Grove T. (2012) Experiments on liquid immiscibility along tholeiitic liquid lines of descent. *Contrib. Mineral. Petr.* **164**, 27–44.

Charlier B., Namur O., Latypov R. and Tegner C. (2015) Layered Intrusions. Springer, pp. 748.

Cherniak D. J. and Dimanov A. (2010) Diffusion in pyroxene, mica and amphibole. *Rev. Mineral. Geochem.* **72**, 641–690.

Chen L.-M., Song X.-Y., Hu R.-Z., Yu S.-Y., Yi J.-N., Kang J. and Huang K.-J. (2021) Mg-Sr-Nd isotopic insights into petrogenesis of the Xiarihamu mafic-ultramafic intrusion, northern Tibetan Plateau, China. *J. Petrol.* **62**.

Chen L.-M., Song X.-Y., Hu R.-Z., Yu S.-Y., He H.-L., Dai Z.-H., She Y.-W. and Xie W. (2017) Controls on trace-element partitioning among co-crystallizing minerals: Evidence from the Panzhihua layered intrusion, SW China. *Am. Mineral.* **102**, 1006–1020.

Chen L.-M., Song X.-Y., Zhu X.-K., Zhang X.-Q., Yu S.-Y. and Yi J.-N. (2014) Iron isotope fractionation during crystallization and sub-solidus re-equilibration: Constraints from the Baima mafic layered intrusion, SW China. *Chem. Geol.* **380**, 97–109.

Chen L.-M., Teng F.-Z., Song X.-Y., Hu R.-Z., Yu S.-Y., Zhu D. and Kang J. (2018) Magnesium isotopic evidence for chemical disequilibrium among cumulus minerals in layered mafic intrusion. *Earth. Planet. Sci. Lett.* **487**, 74–83.

Chen S., Niu Y., Guo P., Gong H., Sun P., Xue Q., Duan M. and Wang X. (2019) Iron isotope fractionation during mid-ocean ridge basalt (MORB) evolution: Evidence from lavas on the East Pacific Rise at 10°30′N and its implications. *Geochim. Cosmochim. Acta* **267**, 227–239.

Dare S., Bethell E. and Barnes S.-J. (2019) Constraining the formation of Fe–Ti–V–P deposits using trace elements in Fe–Ti oxides: insights from the chemostratigraphic variation of magnetite and ilmenite in the Upper Zone of the Bushveld Igneous Complex. *GAC-MAC-IAH Québec 2019*.

Dare S. A. S., Barnes S.-J. and Beaudoin G. (2012) Variation in trace element content of magnetite crystallized from a fractionating sulfide liquid, Sudbury, Canada: Implications for provenance discrimination. *Geochim. Cosmochim. Acta* **88**, 27–50.

Dziony W., Horn I., Lattard D., Koepke J., Steinhoefel G., Schuessler J. A. and Holtz F. (2014) In-situ Fe isotope ratio determination in Fe–Ti oxides and sulfides from drilled gabbros and basalt from the IODP Hole 1256D in the eastern equatorial Pacific. *Chem. Geol.* **363**, 101–113.

Frost B. R. and Lindsley D. H. (1991) Occurrence of iron-titanium oxides in igneous rocks. *Rev. Mineral. Geochem.* **25**, 433–468.

Howarth G. H. and Prevec S. A. (2013) Trace element, PGE, and Sr–Nd isotope geochemistry of the Panzhihua mafic layered intrusion, SW China: Constraints on ore-forming processes and evolution of parent magma at depth in a plumbing-system. *Geochim. Cosmochim. Acta* **120**, 459–478.

Ganino C., Arndt N. T., Zhou M. F., Gaillard F. and Chauvel C. (2008) Interaction of magma with sedimentary wall rock and magnetite ore genesis in the Panzhihua mafic intrusion, SW China. *Miner. Deposit.* **43**, 677–694.

Ganino C., Harris C., Arndt N. T., Prevec S. A. and Howarth G. H. (2013) Assimilation of carbonate country rock by the parent magma of the Panzhihua Fe-Ti-V deposit (SW China): Evidence from stable isotopes. *Geosci. Front.* **4**, 547–554.

Gleeson M. L. M., Gibson S. A. and Williams H. M. (2020) Novel insights from Fe-isotopes into the lithological heterogeneity of Ocean Island Basalts and plume-influenced MORBs. *Earth. Planet. Sci. Lett.* **535**, 116114.

Jang Y. D. and Naslund H. R. (2003) Major and trace element variation in ilmenite in the Skaergaard Intrusion: petrologic implications. *Chem. Geol.* **193**, 109–125.

Jang Y. D., Naslund H. R. and McBirney A. R. (2001) The differentiation trend of the Skaergaard intrusion and the timing of magnetite crystallization: iron enrichment revisited. *Earth. Planet. Sci. Lett.* **189**, 189–196.

Knipping J. L., Fiege A., Simon A. C., Oeser M., Reich M. and Bilenker L. D. (2019) In-situ iron isotope analyses reveal igneous and magmatic-hydrothermal growth of magnetite at the Los Colorados Kiruna-type iron oxide-apatite deposit, Chile. *Am. Mineral.* **104**, 471–484.

Li C.-F., Li X.-H., Li Q.-L., Guo J.-H., Li X.-H. and Yang Y.-H. (2012) Rapid and precise determination of Sr and Nd isotopic ratios in geological samples from the same filament loading by thermal ionization mass spectrometry employing a single-step separation scheme. *Anal. Chim. Acta.* **727**, 54–60.

Lindsley D. H. (1991) Experimental studies of oxide minerals. *Rev. Mineral. Geochem.* **25**, 69–106.

Liu P.-P., Zhou M.-F., Luais B., Cividini D. and Rollion-Bard C. (2014a) Disequilibrium iron isotopic fractionation during the high-temperature magmatic differentiation of the Baima Fe–Ti oxide-bearing mafic intrusion, SW China. *Earth Planet. Sci. Lett.* **399**, 21–29.

Liu P.-P., Zhou M.-F., Chen W. T., Boone M. and Cnudde V. (2014b) Using multiphase solid inclusions to constrain the origin of the Baima Fe–Ti–(V) oxide deposit, SW China. *J. Petrol.* **55**, 951–976.

Liu P.-P., Zhou M.-F., Chen W. T., Gao J.-F. and Huang X.-W. (2015) In-situ LA-ICP-MS trace elemental analyses of magnetite: Fe–Ti–(V) oxide-bearing mafic–ultramafic layered intrusions of the Emeishan Large Igneous Province, SW China. *Ore. Geol. Rev.* **65**, 853–871.

Liu Y. S., Hu Z. C., Gao S., Gunther D., Xu J., Gao C. G. and Chen H. H. (2008) In situ analysis of major and trace elements of anhydrous minerals by LA-ICP-MS without applying an internal standard. *Chem. Geol.* **257**, 34–43.

Luan Y., Sun X.-H., Liu M.-W. and He K. (2021) Analysis method for in-situ trace element determination of magnetite by LA-ICP-MS. *Bull. Geo. Sci. Tech.* **40**, 167–175.

Morse S. A. (1980) Kiglapait mineralogy II: Fe-Ti oxide minerals and the activities of oxygen and silica. *J. Petrol.* **21**, 685–719.

Pang K.-N., Teng F.-Z., Sun Y., Chung S.-L. and Hossein Zarrinkoub M. (2020) Magnesium isotopic systematics of the Makran arc magmas, Iran: Implications for crust-mantle Mg isotopic balance. *Geochim. Cosmochim. Acta* **278**, 110–121.

Pang K. N., Li C. S., Zhou M. F. and Ripley E. M. (2008a) Abundant Fe-Ti oxide inclusions in olivine from the Panzhihua and Hongge layered intrusions, SW China: Evidence for early saturation of Fe-Ti oxides in ferrobasaltic magma. *Contrib. Mineral. Petr.* **156**, 307–321.

Pang K. N., Zhou M. F., Lindsley D., Zhao D. and Malpas J. (2008b) Origin of Fe-Ti oxide ores in mafic intrusions: Evidence from the Panzhihua intrusion, SW China. *J. Petrol.* **49**, 295–313.

Panxi Geological Unit (1984) *Mineralization and exploration forecasting of V-Ti magnetite deposits in the Panzhihua-Xichang region*. Panxi Geological Unit, pp. 279.

Poitrasson F., Zambardi T., Magna T. and Neal C. R. (2019) A reassessment of the iron isotope composition of the Moon and its implications for the accretion and differentiation of terrestrial planets. *Geochim. Cosmochim. Acta* **267**, 257–274.

Richter F. M., Watson E. B., Mendybaev R., Dauphas N., Georg B., Watkins J. and Valley J. (2009) Isotopic fractionation of the major elements of molten basalt by chemical and thermal diffusion. *Geochim. Cosmochim. Acta* **73**, 4250–4263.

Richter F. M., Watson E. B., Mendybaev R. A., Teng F. Z. and Janney P. E. (2008) Magnesium isotope fractionation in silicate melts by chemical and thermal diffusion. *Geochim. Cosmochim. Acta* **72**, 206–220.

Schauble E. A. (2011) First-principles estimates of equilibrium magnesium isotope fractionation in silicate, oxide, carbonate and hexaaquamagnesium(2+) crystals. *Geochim. Cosmochim. Acta* **75**, 844–869.

Schmidt M. W., Connolly J. A. D., Günther D. and Bogaerts M. (2006) Element partitioning: The role of melt structure and composition. *Science* **312**, 1646–1650.

Sedaghatpour F. and Jacobsen S. B. (2018) Magnesium stable isotopes support the lunar magma ocean cumulate remelting model for mare basalts. *Proc. Natl. Acad. Sci. USA* **116**(1), 201811377.

Sedaghatpour F., Teng F.-Z., Liu Y., Sears D. W. G. and Taylor L. A. (2013) Magnesium isotopic composition of the Moon. *Geochim. Cosmochim. Acta* **120**, 1–16.

Shellnutt J. and Pang K.-N. (2012) Petrogenetic implications of mineral chemical data for the Permian Baima igneous complex, SW China. *Miner. Petrol.* **106**, 75–88.

Shellnutt J. G., Zhou M. F. and Zellmer G. F. (2009) The role of Fe-Ti oxide crystallization in the formation of A-type granitoids with implications for the Daly gap: An example from the Permian Baima igneous complex, SW China. *Chem. Geol.* **259**, 204–217.

Song X. Y., Qi H. W., Hu R. Z., Chen L. M., Yu S. Y. and Zhang J. F. (2013) Formation of thick stratiform Fe-Ti oxide layers in layered intrusion and frequent replenishment of fractionated mafic magma: Evidence from the Panzhihua intrusion, SW China. *Geochem. Geophys. Geosyst.* **14**, 712–732.

Sossi P. A., Foden J. D. and Halverson G. P. (2012) Redox-controlled iron isotope fractionation during magmatic differentiation: an example from the Red Hill intrusion, S. Tasmania. *Contrib. Mineral. Petrol.* **164**, 757–772.

Sossi P. A. and O'Neill H. S. C. (2017) The effect of bonding environment on iron isotope fractionation between minerals at high temperature. *Geochim. Cosmochim. Acta* **196**, 121–143.

Su B.-X., Hu Y., Teng F.-Z., Qin K.-Z., Bai Y., Sakyi P. A. and Tang D.-M. (2017) Chromite-induced magnesium isotope fractionation during mafic magma differentiation. *Sci. Bull.* **62**, 1538–1546.

Su B.-X., Hu Y., Teng F.-Z., Xiao Y., Zhang H.-F., Sun Y., Bai Y., Zhu B., Zhou X.-H. and Ying J.-F. (2019) Light Mg isotopes in mantle-derived lavas caused by chromite crystallization, instead of carbonatite metasomatism. *Earth. Planet. Sci. Lett.* **522**, 79–86.

Tang H., Szumila I., Trail D. and Young E. D. (2021) Experimental determination of the effect of Cr on Mg isotope fractionation between spinel and forsterite. *Geochim. Cosmochim. Acta* **296**, 152–169.

Teng F.-Z. (2017) Magnesium isotope geochemistry. *Rev. Mineral. Geochem.* **82**, 219–287.

Teng F.-Z., Dauphas N., Helz R. T., Gao S. and Huang S. (2011) Diffusion-driven magnesium and iron isotope fractionation in Hawaiian olivine. *Earth. Planet. Sci. Lett.* **308**, 317–324.

Teng F.-Z., Dauphas N., Huang S. and Marty B. (2013) Iron isotopic systematics of oceanic basalts. *Geochim. Cosmochim. Acta* **107**, 12–26.

Teng F.-Z., Li W.-Y., Ke S., Marty B., Dauphas N., Huang S., Wu F.-Y. and Pourmand A. (2010) Magnesium isotopic composition of the Earth and chondrites. *Geochim. Cosmochim. Acta* **74**, 4150–4166.

Teng F.-Z., Li W.-Y., Ke S., Yang W., Liu S.-A., Sedaghatpour F., Wang S.-J., Huang K.-J., Hu Y., Ling M.-X., Xiao Y., Liu X.-M., Li X.-W., Gu H.-O., Sio C. K., Wallace D. A., Su B.-X., Zhao L., Chamberlin J., Harrington M. and Brewer A. (2015) Magnesium isotopic compositions of international geological reference materials. *Geostand. Geoanal. Res.* **39**, 329–339.

Teng F.-Z., Wadhwa M. and Helz R. T. (2007) Investigation of magnesium isotope fractionation during basalt differentiation: Implications for a chondritic composition of the terrestrial mantle. *Earth Planet. Sci. Lett.* **261**, 84–92.

Teng F.-Z., Wang S.-J. and Moynier F. (2019) Tracing the formation and differentiation of the Earth by non-traditional stable isotopes. *Sci. China-Earth Sci.* **62**, 1702–1715.

Teng F.-Z. and Yang W. (2014) Comparison of factors affecting the accuracy of high-precision magnesium isotope analysis by multi-collector inductively coupled plasma mass spectrometry. *Rapid Commun. Mass. Space* **28**, 19–24.

Tian H.-C., Yang W., Li S.-G. and Ke S. (2017) Could sedimentary carbonates be recycled into the lower mantle? Constraints from Mg isotopic composition of Emeishan basalts. *Lithos* **292–293**, 250–261.

Tian H.-C., Zhang C., Teng F.-Z., Long Y.-J., Li S.-G., He Y., Ke S., Chen X.-Y. and Yang W. (2020) Diffusion-driven extreme Mg and Fe isotope fractionation in Panzhihua ilmenite: Implications for the origin of mafic intrusion. *Geochim. Cosmochim. Acta* **278**, 361–375.

Toplis M. J. and Carroll M. R. (1995) An experimental study of the influence of oxygen fugacity on Fe-Ti oxide stability, phase relations, and mineral-melt equilibria in ferro-basaltic systems. *J. Petrol.* **36**, 1137–1170.

Van Orman J. A. and Crispin K. L. (2010) Diffusion in oxides. *Rev. Mineral. Geochem.* **72**, 757–825.

Veksler I., Dorfman A., Danyushevsky L., Jakobsen J. and Dingwell D. (2006) Immiscible silicate liquid partition coefficients: implications for crystal-melt element partitioning and basalt petrogenesis. *Contrib. Mineral. Petr.* **152**, 685–702.

Veksler I. V. and Charlier B. (2015) Silicate liquid immiscibility in layered intrusions. In *Layered Intrusions* (eds. B. Charlier, O. Namur, R. Latypov and C. Tegner). Springer, Netherlands, Dordrecht, pp. 229–258.

Wager L. R. and Brown G. M. (1967) *Layered Igneous Rocks*. Oliver and Boyd, Edinburgh.

Wang C. Y. and Zhou M.-F. (2013) New textural and mineralogical constraints on the origin of the Hongge Fe-Ti-V oxide deposit, SW China. *Miner. Deposit.* **48**, 787–798.

Wang K., Wang C. Y. and Ren Z.-Y. (2018) Apatite-hosted melt inclusions from the Panzhihua gabbroic-layered intrusion associated with a giant Fe–Ti oxide deposit in SW China: insights for magma unmixing within a crystal mush. *Contrib. Mineral. Petrol.* **173**, 59.

Watson E. B. and Müller T. (2009) Non-equilibrium isotopic and elemental fractionation during diffusion-controlled crystal growth under static and dynamic conditions. *Chem. Geol.* **267**, 111–124.

Wei Y., Niu Y., Gong H., Duan M., Chen S., Guo P. and Sun P. (2020) Geochemistry and iron isotope systematics of coexisting Fe-bearing minerals in magmatic FeTi deposits: A case study of the Damiao titanomagnetite ore deposit, North China Craton. *Gondwana Res.* **81**, 240–251.

Weis D., Kieffer B., Maerschalk C., Barling J., de Jong J., Williams G. A., Hanano D., Pretorius W., Mattielli N., Scoates J. S., Goolaerts A., Friedman R. M. and Mahoney J. B. (2006) High-precision isotopic characterization of USGS reference materials by TIMS and MC-ICP-MS. *Geochem. Geophys. Geosyst.* **7**, 30.

Xu Y. G., He B., Chung S. L., Menzies M. A. and Frey F. A. (2004) Geologic, geochemical, and geophysical consequences of plume involvement in the Emeishan flood-basalt province. *Geology* **32**, 917–920.

Yu S.-Y., Song X.-Y., Ripley E. M., Li C., Chen L.-M., She Y.-W. and Luan Y. (2015) Integrated O-Sr–Nd isotope constraints on the evolution of four important Fe–Ti oxide ore-bearing mafic–ultramafic intrusions in the Emeishan large igneous province, SW China. *Chem. Geol.* **401**, 28–42.

Zhang X.-Q., Song X.-Y., Chen L.-M., Xie W., Yu S.-Y., Zheng W.-Q., Deng Y.-F., Zhang J.-F. and Gui S.-G. (2012) Fractional crystallization and the formation of thick Fe–Ti–V oxide layers in the Baima layered intrusion, SW China. *Ore Geol. Rev.* **49**, 96–108.

Zhang X. Q., Song X. Y., Chen L. M., Yu S. Y., Xie W., Deng Y. F., Zhang J. F. and Gui S. G. (2013) Chalcophile element geochemistry of the Baima layered intrusion, Emeishan large igneous province, SW China: Implications for sulfur saturation history and genetic relationship with high-Ti basalts. *Contrib. Mineral. Petrol.* **166**, 193–209.

Zhao X.-M., Zhang H.-F., Zhu X.-K., Zhu B. and Cao H.-H. (2015) Effects of melt percolation on iron isotopic variation in peridotites from Yangyuan, North China Craton. *Chem. Geol.* **401**, 96–110.

Zhou M.-F., Chen W. T., Wang C. Y., Prevec S. A., Liu Patricia P. and Howarth G. H. (2013) Two stages of immiscible liquid separation in the formation of Panzhihua-type Fe-Ti-V oxide deposits, SW China. *Geosci. Front.* **4**, 481–502.

Zheng W.-Q., Deng Y.-F., Song X.-Y., Chen L.-M., Yu S.-Y., Zhou G.-F., Liu S.-R. and Xiang J.-X. (2014) Composition and genetic significance of the ilmenite of the Panzhihua intrusion. *Acta Petrol. Sin.* **30**, 1432–1442.

Zhou M. F., Arndt N. T., Malpas J., Wang C. Y. and Kennedy A. K. (2008) Two magma series and associated ore deposit types in the Permian Emeishan large igneous province, SW China. *Lithos* **103**, 352–368.

Zhou M. F., Robinson P. T., Lesher C. M., Keays R. R., Zhang C. J. and Malpas J. (2005) Geochemistry, petrogenesis and metallogenesis of the Panzhihua gabbroic layered intrusion and associated Fe-Ti-V oxide deposits, Sichuan Province, SW China. *J. Petrol.* **46**, 2253–2280.

Zhu D., Bao H. and Liu Y. (2015) Non-traditional stable isotope behaviors in immiscible silica-melts in a mafic magma chamber. *Sci. Rep.* **5**, 17561.

Associate editor: Shichun Huang